

***In vivo* imaging of transplanted stem cells with advanced
functional nanoparticles for regenerative medicine**

2016

Yusuke Ogihara

CONTENTS

Chapter 1 General introduction

Chapter 2 Interaction of stem cells with lymphomononuclear cells (LMCs)

2.1 Introduction

2.2 Materials and methods

2.2.1 The isolation and culture of adipose-derived stem cells (ASCs)

2.2.2 Flow cytometric analysis of ASCs

2.2.3 The isolation of murine LMCs

2.2.4 Effect of ASCs on LMCs proliferation

2.2.5 Analysis of Population Rate of LMCs co-cultured with ASCs

2.2.6 Quantitative production analysis of hormone and growth factor

2.2.7 Quantitative real-time reverse-transcription polymerase chain reaction

(qRT-PCR) nalysis for Cytokines, Chemokines and Cell Surface Markers

2.3 Results and discussion

2.3.1 Characteristics of ASCs

2.3.2 Suppressive effects of ASCs on LMCs proliferation

2.3.3 Change of cell population in LMCs co-cultured with ASCs

2.4 Conclusion

Chapter 3 The influence of ASCs on the treatment of fulminant hepatic failure (FHF)

3.1 Introduction

3.2 Materials and methods

3.2.1 Animals

3.2.2 Experimental models of acute liver injury and treatment with ASCs

3.2.3 Measurement of liver enzymes

3.2.4 qRT-PCR analysis for cytokines, chemokines and cell surface markers

3.3 Results and discussion

3.3.1 Effects of transplanted ASCs on Con A-induced liver injury

3.3.2 Cytokines and cell surface lineage markers expressed in the Injured Liver

3.4 Conclusion

Chapter 4 Transduction of octa-arginine (R8)- ZnS-ZAIS-COOH (ZZC) into ASCs

4.1 Introduction

4.2 Materials and methods

- 4.2.1 The synthesis of ZnS-coated ZAIS (ZnS-ZAIS) nanoparticles
- 4.2.2 The particle properties analysis
- 4.2.3 The transduction of R8-ZZC into ASCs

4.3 Results and discussion

- 4.3.1 The properties of ZZC and R8-ZZC
- 4.3.2 The fluorescence stability of R8-ZZC in cell culture medium
- 4.3.3 The optimal concentration ratio of ZZC and R8

4.4 Conclusion

Chapter 5 The evaluation R8-ZZC labeled ASCs

5.1 Introduction

5.2 Materials and methods

- 5.2.1 The cytotoxicity test of R8-ZZC to ASCs
- 5.2.2 The proliferation of R8-ZZC labeled ASCs
- 5.2.3 Adipogenic and osteogenic differentiation
- 5.2.4 The measurement of inflammation markers

5.3 Results and discussion

- 5.3.1 The cytotoxicity of R8-ZZC to ASCs
- 5.3.2 The inflammatory cytokine production of R8-ZZC-labeled ASCs
- 5.3.3 The differentiation of R8-ZZC-labeled ASCs

5.4 Conclusion

Chapter 6 *In vivo* and *ex vivo* imaging of R8-ZZC-labeled ASCs

6.1 Introduction

6.2 Materials and methods

- 6.2.1 The observation of R8-ZZC-labeled ASCs in the mice
- 6.2.2 The observation of R8-ZZC-labeled ASCs in the organs
- 6.2.3 Multiphoton analysis

6.3 Results and discussion

- 6.3.1 Relevance of fluorescence intensity to cell numbers

6.3.2 *Ex vivo* fluorescence imaging of the transplanted R8-ZZC-labeled ASCs

6.4 Conclusion

Chapter 7 Transduction of quantum dots (QDs) and magnetic nanoparticles (TMADM) into ASCs

7.1 Introduction

7.2 Materials and methods

7.2.1 The transduction efficiency of QDs-TMADM to ASCs

7.2.2 Fluorescence and TEM analysis

7.2.3 The cytotoxicity of QDs-TMADM to ASCs

7.2.4 The proliferation of ASCs labeled with QDs-TMADM

7.3 Results and discussion

7.3.1 The optimal concentration ratio of QDs and TMADM

7.3.2 The evaluation of ASCs labeled with QDs-TMADM

7.4 Conclusion

Chapter 8 *In vitro* and *in vivo* imaging of ASCs labeled with QDs-TMADM-03

8.1 Introduction

8.2 Materials and methods

8.2.1 *In vitro* imaging of ASCs labeled with QDs-TMADM

8.2.2 *In vivo* imaging of ASCs labeled with QDs-TMADM

8.2.3 Multi color imaging of ASCs labeled with QDs-TMADM

8.3 Results and discussion

8.3.1 *In vitro* imaging of ASCs by magnetic resonance and fluorescence imaging

8.3.2 *In vivo* imaging of ASCs in

8.4 Conclusion

Chapter 9 Concluding remarks

Acknowledgements

References

List of publications

Chapter 1 General introduction

Stem cell therapy plays an important role in regenerative medicine, especially for tissues and organs that are difficult to reconstruct due to their complicated structures and functions such as the guts, liver and islets¹⁻³. Numerous types of somatic stem cells have been established thus leading to numerous medical applications in regenerative medicine, because their stem cells have been already confirmed to be safe in comparison to embryonic stem (ES) cells and induce induced pluripotent stem (iPS) cells⁴⁻⁷. Adipose tissue-derived stem cells (ASCs) have received a great deal of attention in recent years as multipotent somatic stem cells. Large amount of ASCs can be obtained using methods that are relatively easy to perform such as lipoaspiration under local anesthesia. These cells have the ability to self-renew and to efficiently differentiate in various types of mesenchymal cells, including adipocytes and osteocytes^{8,9}.

Acute liver failures including fulminant hepatic failure (FHF) are incurable diseases with significant morbidity and mortality. The pathological basis of FHF is massive destruction of hepatocytes due to excessive immune responses provoked by viral infection, autoimmunity or chemical reactions in the liver. Therefore, the inhibition of the excessive immune responses is extremely important for the treatment of FHF. If patients do not receive prompt and appropriate treatments, FHF progresses rapidly toward death^{10,11,12}. ASCs, due to low the regulatory hurdles of clinical applications, may be a good candidate for the source of cell therapies of FHF with excessive immune responses. However, the immunomodulatory effects of ASCs on the excessive immune responses in FHF remain poorly understood. The development of technologies to label and image ASCs has therefore become important in making further progress in their clinical applications.

Quantum dots (QDs) are inorganic fluorescence probes that have many distinctive advantages in comparison to organic or protein fluorescence probes, including high luminance, superior photostability, high quantum yields and wide excitation wavelengths^{13,14}. Based on these characteristics, QDs have recently received a great deal of attention as fluorescence probes for biomolecules and live cells, including stem cells¹⁵. Yukawa *et al.*, has developed QD labeling methods for stem cells using cationic liposomes and octa-arginine (R8) peptides (also known as cell-penetrating peptides)^{16,17}.

However, well-developed QDs contain toxic elements, including (but not limited to) Cd, Pb, Hg, Se and Te. Thus, the development of novel QDs with extremely low cytotoxicity (especially Cd-free alternatives) is necessary for further advancement of QD technology¹⁸⁻²¹. Torimoto *et al.* previously reported the facile synthesis of ZnS-AgInS₂ (ZAIS) as a cadmium-free QD, and confirmed that ZAIS was useful as a color-adjustable fluorophore mainly for solar cells^{22,23}. ZAIS exhibited intense fluorescence from about 500 nm to 800 nm (which includes near-infrared region) at room temperature, when the composition rate of AgIn and Zn were changed in the ZAIS nanoparticles. At present the biological application of ZAIS, especially stem cell labeling and *in vivo* imaging remains largely uninvestigated²⁴⁻²⁷.

In the present study, ZnS-coated ZAIS (ZnS-ZAIS) nanoparticles was carboxylated in order to allow for its dispersal in aqueous solutions such as phosphate buffered saline (PBS) and cell culture medium. Then, the fluorescence labeling of ASCs by ZnS-ZAIS carboxylated nanoparticles (ZZC) and R8 complex (R8-ZZC) was then addressed. The influence of R8-ZZC labeling on the properties of ASC, especially in regard to the induction of major inflammatory cytokines, was investigated, and *in vivo* fluorescence imaging of transplanted R8-ZZC-labeled ASCs was performed in mice. I also investigated the accumulation of transplanted ASCs using high-speed multiphoton confocal laser microscopy.

I also focus on Magnetic resonance imaging (MRI) which is the technique that already used *in vivo* imaging. The image contrast of MRI is higher than CT and there is no exposure to body^{28,29}. MRI has the high penetration depth and clinical availability. MRI method can be used together with magnetic nanoparticles²⁸⁻³¹.

For transducing magnetic nanoparticles, transduction methods with protein were developed. In previous reports, we showed that positively charged nanoparticles [trimethylamino dextran-coated magnetic iron oxide nanoparticles (TMADM)], in which exists the cationic end-group substitution of dextran, could be transduced into the mouse insulinoma 6 (MIN6) b-cell line³². And Yukawa H. *et al.* synthesized TMADM nanoparticles and observed them inside three-dimensional (3D) human hepatocellular carcinoma cells (HepG2; liver hepatocellular carcinoma-derived cell line) spheroids, which mimic an environment close to natural tissues using Cellable™ plates³³. Those results suggested that TMADM was efficiently incorporated into cells (CM-5-89).

The transduction efficiency of TMADM into ASCs was about four-fold more efficient than that of the alkali-treated dextran-coated magnetic iron oxide nanoparticle (ATDM), which is a major component of commercially available contrast agents such as ferucarbotran (Resovist), and the level of labeling was maintained for at least two weeks³⁴.

TMADM has proven to be stably dispersed in the culture medium including fetal bovine serum, and is efficient for labeling mature cells without exerting cytotoxic effect. In this study, I investigated the usefulness of QDs conjugated TMADM for observation of the transplanted ASCs. I developed multimodal imaging method using MRI and fluorescence imaging.

Chapter 2 Interaction of stem cells with lymphomononuclear cells (LMCs)

2.1 Introduction

Recently, cell transplantation therapy using adipose tissue-derived stem cells (ASCs) has received much attention, because ASCs possess immunomodulatory properties as well as multilineage differentiation ability³⁵⁻⁴³. Considering the clinical application of cell therapy, ASCs have several advantages in comparison to mature cells or other stem cells. ASCs could be prepared by minimal invasive procedure: removing and processing subcutaneous fat in which precursors of ASCs are frequently included. They have proved to grow faster *in vitro* and to produce various cytokines and growth factors relating to their immunomodulatory effects more abundantly, in comparison to other mesenchymal stem cells (MSCs)^{44,45}. In addition, the regulatory hurdles of clinical applications for ASCs are substantially lower than those for embryonic stem (ES) cells or induced pluripotent stem (iPS) cells. Thus, ASCs may be a good candidate for the source of cell therapies of fulminant hepatic failure (FHF) with excessive immune responses. However, the immunomodulatory effects of ASCs on the excessive immune responses in FHF remain poorly understood.

Three kinds of mitogens are known to influence the proliferation of lymphomononuclear cells (LMCs) *in vitro*, which are phorbol 12-myristate 13-acetate (PMA) plus ionomycin [for the activation of both T cells and B cells by protein kinase C (PKC) phosphorylation], concanavalin A (Con A) [for the activation of T cells by indirect activation T cell receptor (TCR) cross-linking], and lipopolysaccharide (LPS) [for the activation of B cells by Toll-like receptor (TLR)4/myeloid differentiation factor (MD)2, cluster of differentiation 180 (CD180)/MD1 activation]. In addition, a number of animal models for acute liver failures including FHF have been reported until present, such as Con A-induced, galactosamine/lipopolysaccharide-induced, carbon tetrachloride (CCl₄)-induced liver injury, and so on⁴⁶⁻⁵⁰. Con A-induced liver injury has been used as a representative model for acute liver failure including FHF, because the pathogenic mechanism of liver injury is principally immune-dependent and well-characterized. In Con A-induced liver injury, T cells and natural killer T (NKT) cells are thought to be primarily activated by Con A, and cytokines produced by these activated cells, such as tumor necrosis factor- α (TNF- α) and interferon- γ (IFN- γ), are considered to act as exacerbating factors⁵¹⁻⁵³. Moreover, the damaged hepatocytes generate free radicals, thereby activating Kupffer cells (liver

macrophages) to produce various cytokines that accelerate progression of liver inflammation^{54,55}.

In this study, I assessed the effect of ASCs on the inhibition of the proliferation of LMCs *in vitro* using three kinds of mitogens, such as PMA plus ionomycin, LPS and Con A.

2.2 Materials and methods

2.2.1 The isolation and culture of adipose-derived stem cells (ASCs)

Subcutaneous adipose tissues were taken from 6- to 8-wk-old C57BL/6 mice and placed in Dulbecco's modified Eagle's medium (DMEM, Wako Pure Chemical Industries Ltd, Osaka, Japan) containing 10% fetal bovine serum (FBS, Thermo Scientific HyClone, Logan, Utah, USA), minced finely with adding 1mL Hank's balanced salt solution (HBSS, Life Technologies, Grand Island, NY, USA). The minced tissues were incubated in 10 mL HBSS containing 0.1% collagenase (type I, Worthington Biochemical Co, Lakewood, NJ, USA) at 37°C for 60 min. Cells were collected from digested tissue through 100 µm-mesh after being suspended in DMEM. After centrifugation at 300 × g for 10 min, the precipitated cells were washed twice with DMEM, and resuspended in a culture medium containing 20% FBS as described below. Then the cells were seeded in fibronectin-coated 75 cm² flasks, and attached fibroblast-like cells were cultured as the progenitors of ASCs. The basal medium was 3:2 mixture of DMEM and MCDB 201 medium (Sigma Aldrich, St Louis, MO, USA), supplemented with 1 ng/mL linoleic acid-albumin (Sigma Aldrich), 1 × insulin, transferrin, selenium (ITS) supplement (Sigma Aldrich), 0.1 mM ascorbic acid phosphate ester magnesium salt (Wako Pure Chemical Industries), 50 U/mL penicillin and 50 mg/mL streptomycin (Wako Pure Chemical Industries) and 10 ng/mL human fibroblast growth factor-2 (FGF-2) (Peprotech, Inc., Rocky Hill, NJ, USA).

2.2.2 Flow cytometric analysis of ASCs

ASCs were incubated with antibodies for 30 min on ice. The antibodies used for detecting cell surface markers were as follows; phycoerythrin (PE)-conjugated anti-mouse CD29, CD105, lymphocyte antigen 6A/E (Ly-6A/E; also known as stem cell antigen-1 or Sca-1) antibodies (BD Biosciences, Tokyo, Japan), fluorescein isothiocyanate (FITC)-conjugated anti-mouse CD45, CD90, CD117 antibodies (BD Biosciences) and allophycocyanin (APC)-conjugated anti-mouse CD44 antibodies

(BD). CD45 is a marker for pan-hematopoietic cells. CD29 (β 1 integrin) and CD44 (phagocytic glycoprotein-1) are adhesion molecules, and used as markers for MSCs. CD90 (Thy-1) and CD105 (Endoglin) are markers for a variety of stem cells including MSCs. PE-, FITC-, and APC-conjugated rat IgG (BD Biosciences) were used as isotype controls. Flow cytometry was performed using fluorescence activate cell sorter (FACS) Caliber (BD Biosciences).

2.2.3 The isolation of murine LMCs

Spleens from sacrificed mice (C57BL/6) were minced, and washed with Roswell Park Memorial Institute (RPMI) 1640 (Sigma Aldrich). After lysing erythrocytes with Tris NH_4Cl , the splenocytes served as LMCs. The LMCs were counted, and then resuspended at the concentration of $2-4 \times 10^6$ viable cells/mL in a complete medium.

2.2.4 Effect of ASCs on LMCs proliferation

To analyze the influence of ASCs on LMC proliferation, murine LMCs (2×10^5 cells) were seeded in a 96-well plate containing RPMI1640 with 10% FBS, 50 U/mL penicillin and 50 mg/mL streptomycin. They were stimulated with 50 ng/mL PMA (Sigma Aldrich) plus 1 $\mu\text{g}/\text{mL}$ ionomycin (Sigma Aldrich), 5 $\mu\text{g}/\text{mL}$ Con A, or 10 $\mu\text{g}/\text{mL}$ LPS (Sigma Aldrich). The ratios of ASCs to LMCs were 1:10, 1:20, 1:40 and 1:80 in the co-culture condition. After 48 h incubation, the LMCs were collected and seeded in a 96-well plate, and then subjected to bromodeoxyuridine (BrdU) incorporation assay (Roche diagnostics Japan, Tokyo, Japan) according to the manufacturer's instructions. The chemiluminescence of the individual wells was measured using the Wallac 1420 multi-label counter (PerkinElmer Japan Co Ltd, Yokohama, Japan).

To examine the influence of soluble factors produced by ASCs, murine LMCs (2×10^5 cells) stimulated with PMA plus ionomycin, Con A, or LPS were cultured in the culture supernatants of ASC (1×10^5 cells). After 48 h of incubation, the cells were subjected to BrdU incorporation assay (Fig. 2A).

2.2.5 Analysis of Population Rate of LMCs co-cultured with ASCs

To examine the cell population of LMCs co-cultured with ASCs, flow cytometric analysis was performed. Culture and stimulation conditions were the same as the BrdU incorporation assay. After 72 h of incubation, LMCs were labeled with FITC-

conjugated anti-mouse CD3, CD19 antibody (eBioscience Inc, CA, USA), or PE-conjugated natural killer 1.1. (NK1.1) antibody (eBioscience). PE-, FITC-conjugated rat and mouse IgG (BD) were used as isotype controls, respectively. Flow cytometry was performed using FACS Caliber (BD). Simultaneously, viable and dead cells were counted by visualizing dead cells with trypan blue staining (Sigma Aldrich).

2.2.6 Quantitative production analysis of hormone and growth factor

The media of passage 3 ASCs at about 90% confluence were replaced with fresh DMEM containing 10% FBS. After 24 h incubation, the culture media were collected and used for the analysis of hormone/growth factor levels using commercially available enzyme-linked immunosorbent assay (ELISA) kits: Quantikine Mouse hepatocyte growth factor (HGF) or vascular endothelial growth factor (VEGF) Immunoassay (R&D Systems, Minneapolis, MN, USA) for HGF or VEGF detection, and Mouse Prostaglandin E2 (PGE2) ELISA kit (Cusabio Biotech Co Ltd, Wuhan, China) for PGE2 detection. The assays were conducted according to the manufacturer's instructions.

2.2.7 Quantitative real-time reverse-transcription polymerase chain reaction (qRT-PCR) Analysis for Cytokines, Chemokines and Cell Surface Markers

The qRT-PCR was performed using total RNA prepared from ASCs with an RNeasy minikit (Qiagen, Tokyo, Japan). The RNA was subjected for first-strand cDNA synthesis using PrimeScript RT Master Mix (Takara Bio Inc, Shiga, Japan) according to the manufacturer's instructions. Then, qRT-PCR was performed with ABI PRISM 7000 sequence detection system (Applied Biosystems Japan Ltd, Tokyo, Japan) using SYBR Premix DimerEraser (Takara Bio) according to the manufacturer's instructions. The PCR amplification was performed as follows; an initial denaturing step, 95 °C for 30 s; followed by 45 cycles of 95 °C for 5 s, 55 °C for 30 s, and 72 °C for 31 s. Cytokines and chemokine analyzed were as follows; interleukin (IL)-1 α , IL-4, IL-6, IL-10, interferon (IFN)- γ , tumor necrosis factor(TNF)- α , transforming growth factor (TGF)- β , C-X-C motif chemokine 12 (CXCL12)/stromal cell-derived factor (SDF)-1, inducible nitric oxide synthase (iNOS), indoleamine 2, 3-dioxygenase (IDO)1, CD3 γ , CD4, CD8, CD11b and CD11c. Glyceraldehyde 3-phosphate dehydrogenase (GAPDH) was used as an internal control. All the primers were synthesized by Takara Bio Inc (Table 1).

Table 1
Primer sequences used for real-time RT-PCR

Gene	Sense primer	Antisense primer
<i>GAPDH</i>	5'-TGTGTCCGTCGTGGATCTGA-3'	5'-TTGCTGTTGAAGTCGCAGGAG-3'
<i>IL-1a</i>	5'-TGGTTAAATGACCTGCAACAGGAA-3'	5'-AGGTCGGTCTCACTACCTGTGATG-3'
<i>IL-4</i>	5'-ACGGAGATGGATGTGCCAAAC-3'	5'-AGCACCTTGAAGCCCTACAGA-3'
<i>IL-6</i>	5'-CCACTTCACAAGTCGGAGGCTTA-3'	5'-CCAGTTTGGTAGCATCCATCATTTC-3'
<i>IL-10</i>	5'-GCCAGAGCCACATGCTCCTA-3'	5'-GATAAGGCTTGGCAACCCAAGTAA-3'
<i>IFN-γ</i>	5'-CGGCACAGTCATTGAAAGCCTA-3'	5'-GTTGCTGAGGCCTGATTGTC-3'
<i>TNF</i>	5'-TATGGCCAGACCCTCACA-3'	5'-GGAGTAGACAAGGTACAACCCATC-3'
<i>TGF-β</i>	5'-GTGTGGAGCAACATGTGGAACCTA-3'	5'-CGCTGAATCGAAAGCCCTGTA-3'
<i>NOS2</i>	5'-CAAGCTGAACTTGAGCGAGGA-3'	5'-TTTACTCAGTGCCAGAAGCTGGA-3'
<i>CD3g</i>	5'-CTGGGCAACAATGCCAAAGA-3'	5'-AGCCGGATATGGTGCCTATGTTTA-3'
<i>CD4</i>	5'-CAACCTGACTCTGACTCTGGACAA-3'	5'-AGGTAGGTCCCATCACCTCACA-3'
<i>CD8a</i>	5'-GTACTTCAGTTCTGTCTGTCGTCAGTC-3'	5'-TCGCAGCACTGGCTTGGTA-3'
<i>CD11b</i>	5'-CCACTCATTGTGGGCAGCTC-3'	5'-GGGCAGCTTCATTCATCATGTC-3'
<i>CD11c</i>	5'-AGGTCTGCTGCTGCTGGCTA-3'	5'-GGTCCCGTCTGAGACAAACTG-3'

2.3 Results and discussion

2.3.1 Characteristics of ASCs

To confirm the characterization of ASCs, I analyzed cell surface markers, cytokine/chemokine expression patterns, and hormone/growth factor production of ASCs using flow cytometry, Quantitative real-time reverse-transcription polymerase chain reaction (qRT-PCR), and ELISA, respectively. As shown in Fig. 1A, the expressions of CD29, CD44, CD90, CD105 and Sca-1 on ASCs were observed, while the expressions of CD45, CD73, and CD117 were not observed in ASCs; these results are mostly consistent with those of the previous reports^{56,57}. The production of HGF, VEGF, and PGE2 was examined by ELISA using supernatants of ASC cultures, and all of these were confirmed to be produced by ASCs⁵⁷ (Fig. 1B). Moreover, mRNA

expressions of IL-1 α , IL-10, TNF- α , CXCL12/SDF-1, TGF- β , IDO1 and iNOS were examined by qRT-PCR using cellular RNA extracts of ASCs. It is of note that the expressions of cytokines with immunomodulatory functions, such as IL-10 and TGF- β were detected in the examined ASCs, consistent with the previous reports^{56,59} (Fig. 1C). These data suggested that the cells established from C57BL/6 mice have characteristics of ASCs with immunomodulatory functions.

2.3.2 Suppressive effects of ASCs on LMCs proliferation

The suppressive effects of ASCs on the proliferation of LMCs stimulated by PMA plus ionomycin, Con A, or LPS were assessed by BrdU incorporation assay (Fig. 2A). Although the number of ASCs co-cultured with LMCs were relatively small (ASCs:LMCs = 1:80, 1:40, 1:20, 1:10), the proliferation of LMCs was efficiently suppressed in a dose-dependent manner by ASCs in the cases of PMA plus ionomycin-, and Con A-stimulation. On the other hand, this suppressive effect of ASCs on the proliferation of LMCs was not observed in the LPS-stimulated case (Fig. 2B-a,b).

Moreover, I investigated whether intercellular communication was necessary for the immunosuppressive effects of ASCs, and found out that addition of ASC supernatants to LMCs stimulated by each mitogen, did not affect the proliferation of LMCs in 1 and 3 d cultures (Fig. 2C). The results suggest that the direct interaction between ASCs and LMCs is necessary for ASCs to exert suppressive effect on LMC proliferation.

To rule out the possibility that the suppression of LMC proliferation was related to the death of LMCs co-cultured with ASCs, the number of viable and dead LMCs were counted in the co-culture with ASCs (ASC:LMCs = 1:20). In the culture without stimulation, the number of live LMCs was mostly the same regardless of the presence of ASCs, while the number of dead LMCs was decreased in the presence of ASCs. In the culture with Con A stimulation, the number of live and dead LMCs was dramatically increased, while the number of live and dead LMCs were decreased in the presence of ASCs. The results indicate that the inhibitory effect of ASCs on LMC proliferation is not due to the induction of cell death of LMCs (Fig. 3A).

2.3.3 Change of cell population in LMCs co-cultured with ASCs

To examine the changes of cell population of LMCs with or without co-culture with ASCs and Con A stimulation, the cultured LMCs were subjected to the flow cytometric analysis. The levels of the CD3⁺ population (T-cell marker) in the LMCs without Con A stimulation were about 15-20% regardless of the co-culture with ASCs, whereas those with Con A stimulation were more than 40%, showing dramatic increase compared to those without stimulation. In the LMCs stimulated with Con A, the level of the CD3⁺ population was decreased by the co-culture with ASCs.

On the other hand, the CD19⁺ population (B-cell marker) in LMCs remained at the same level in all the culture conditions. The levels of the NK1.1⁺ population (NK-cell marker) in LMCs without Con A stimulation was lower than 5%, and further decreased with Con A stimulation. The levels of the NK1.1⁺ population were unchanged regardless of the co-culture with ASCs. These data suggest that Con A stimulation contributes to the increase of the number of T-cells in LMCs, and ASCs may have the ability to inhibit the proliferation of T-cells or the stimulated cells in LMCs (Fig. 3B).

2.4 Conclusion

The expression of surface CD markers of the isolated ASCs was analyzed using flow cytometry, and they were confirmed to be mostly consistent with those of previous reports^{56,57}. The patterns of cytokine expression and growth factor/hormone production of ASCs were also consistent with those of previous reports⁵⁸. In addition, the differentiation efficiency of ASCs such as for adipocytes and osteocytes could be ascertained comparable to that of previous studies (data not shown). Thus these data suggest that the established cells in the current study possess most of the feature of ASCs as previously reported.

In the current study, ASCs were confirmed to suppress the proliferation of LMCs stimulated with PMA plus ionomycin (T- and B-cell stimulus) and Con A (T-cell stimulus). However, this suppressive effect of ASCs on LMC proliferation was not observed in the case of LPS stimulation (B-cell stimulus). In addition, through the experiment adding culture supernatant of ASCs to LMC culture instead of co-culture with ASCs, it was suggested that the soluble substances such as cytokines and hormones were not responsible for this effect, and that direct interaction between ASCs and LMCs was required for exertion of this suppressive function.

It was confirmed that the suppression of LMC proliferation was not due to the death of LMCs. Furthermore, in the case of Con A-stimulation which leads to T cell proliferation, the rate of T cells in LMCs was tended to be decreased by the co-culture with ASCs. These data suggested that ASCs may mainly affect T cells or the stimulated cells without inducing death to these cells. Since the mechanisms of these effects of ASCs have not yet been elucidated to date, additional analyses for the immunosuppressive function of ASCs, including the necessity of direct interaction to the target cells and specificity to the target cells, are necessary.

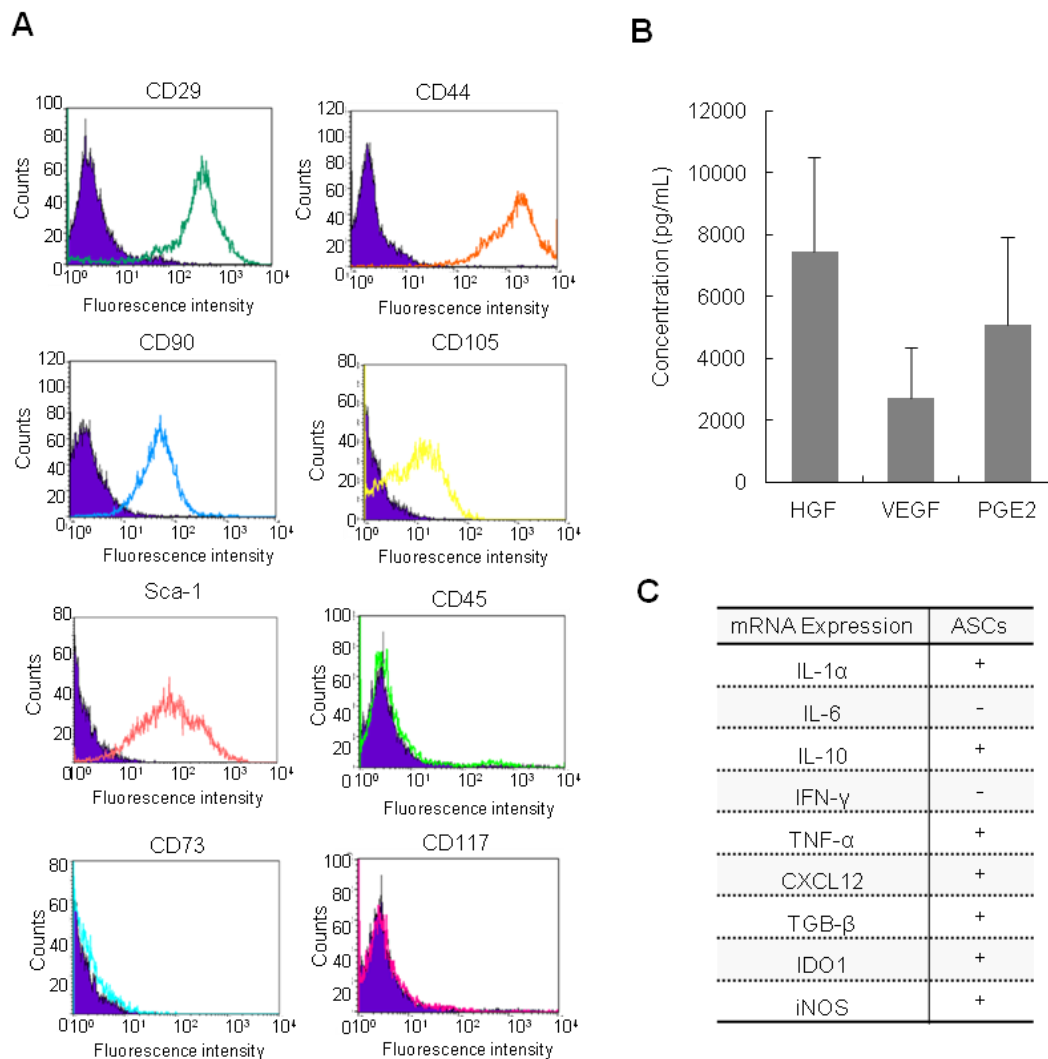


Fig. 1. Characteristics of adipose tissue-derived stem cells (ASCs)

A: Cell surface markers of ASCs analyzed by flow cytometry. The assays were performed in triplicate. CD29: cluster of differentiation 29; Sca-1: stem cell antigen-1; B: The concentrations of hepatocyte growth factor (HGF), vascular endothelial growth factor (VEGF) and prostaglandin synthase E2 (PGE2) produced by ASCs

incubated for 24 h in the culture medium (n = 5). The data are shown as mean \pm SD values. C: The expression of cytokines and chemokines in ASCs analyzed by qPCR. IL-1: interleukin 1; IFN: interferon; TNF: tumor necrosis factor; CXCL12: chemokine C-X-C motif ligand 12; TGF: transforming growth factor; IDO1: indoleamine 2, 3-dioxygenase; iNOS: inducible nitric oxide synthase.

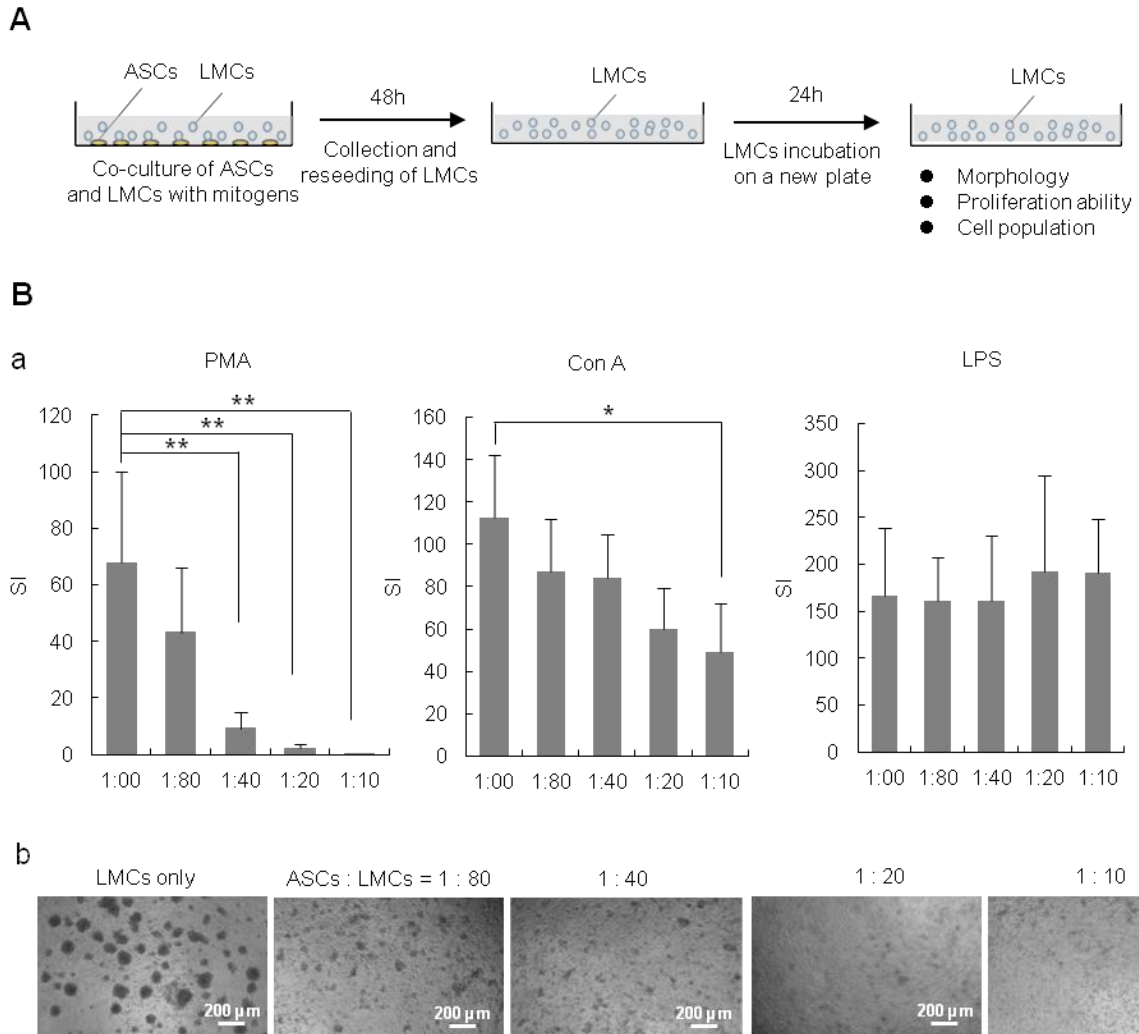


Fig. 2. Effect of ASCs and the culture supernatant on LMC proliferation

A: The scheme of in vitro experiment. Murine lymphomononuclear cells (LMCs) of 2×10^5 /well were placed in a 96-well plate. They were stimulated with phorbol 12-myristate 13-acetate (PMA) 50 ng/mL plus ionomycin 1 μ g/mL, concanavalin A (Con A) 5 μ g/mL, or lipopolysaccharide (LPS) 10 μ g/mL with or without ASCs. In the co-culture case, the ratios of ASCs to LMCs were 1 : 10, 1 : 20, 1 : 40 and 1 : 80. To examine the influence of soluble factors produced by ASCs, LMCs (2×10^5 cells) stimulated with PMA plus ionomycin, Con A, or LPS were cultured for 24 h in the culture supernatants of ASCs (1×10^5 cells/well in 24-well plate). After 48 h of incubation, the LMCs were collected and replated in a 96-well plate, and subjected to bromodeoxyuridine (BrdU) incorporation assay according to the manufacturer's instructions. The chemiluminescence of the individual wells was measured using the Wallac 1420 multi-label counter. B: The proliferation ability (a) and the morphologies

(b) of LMCs stimulated with Con A, PMA plus ionomycin and LPS under co-culture with ASCs. The ratios of ASCs and LMCs were 1:80, 1:40, 1:20 and 1:10. Immunosuppressive effects of murine ASCs on stimulated LMCs were evaluated by BrdU incorporation assay. C: The proliferation ability of LMCs stimulated with Con A, PMA plus ionomycin and LPS under culturing in supernatant from ASCs cultured for 24 h. After 48 h of incubation, BrdU incorporation assay of LMCs were performed. The data are shown at the means \pm SD values (*; $p < 0.05$ and **; $p < 0.001$).

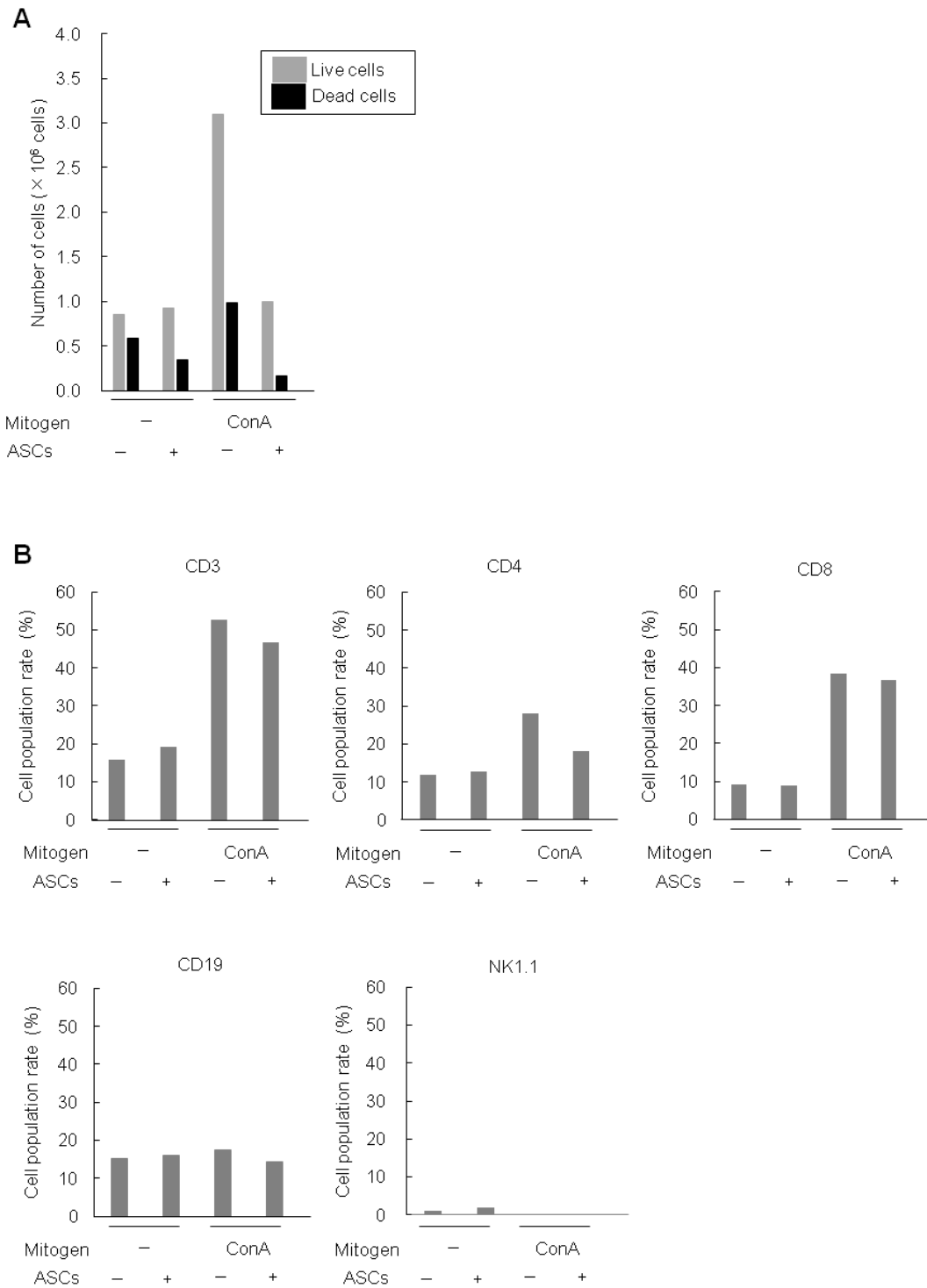


Fig. 3. Viability and cell population changes of LMCs co-cultured with ASCs

A: The number of viable and dead LMCs co-cultured with ASCs. The LMCs were cultured with ASCs in the same condition as the case of the proliferation assay (ASC-to-splenocyte ratio, 1:20) and counted after 48 h of co-culture. B: The cell population changes of mitogen-stimulated LMCs co-cultured with ASCs by flow cytometric

analysis. Culture and stimulation conditions were the same as the BrdU incorporation assay. NK1.1: Natural killer 1.1

Chapter 3 The influence of ASCs on the treatment of fulminant hepatic failure (FHF)

3.1 Introduction

In Chapter 2, the therapeutic efficacy of adipose-derived stem cells (ASCs) for ConA-induced hepatitis was demonstrated. I show that ASCs may affect T cells or the stimulated cells without inducing death to these cells. I therefore hypothesized that ASCs would be able to inhibit the activation of T cells in a mouse model of ConA-induced hepatitis leading to a reduction of liver injury and mortality. The elucidation of ASCs effects *in vivo* has therefore become important in making further progress in their clinical applications.

In this chapter, I examined the therapeutic effects of transplanted ASCs on fulminant hepatic failure (FHF) with excessive immune responses using Con A-induced acute liver failure mice. Through these analyses, I evaluated the therapeutic efficacy of ASCs on acute liver failures including FHF.

3.2 Materials and methods

3.2.1 Animals

C57BL/6 mice were housed in a controlled environment and fed a standard diet with water *ad libitum*. All conditions and handling of animals in this study were conducted under protocols approved by the Nagoya University Committee on Animal Use and Care (#025-018).

3.2.2 Experimental models of acute liver injury and treatment with ASCs

Eight- to ten-week-old male C57BL/6 mice were treated with overnight food/water deprivation, and were injected intravenously with 15 mg/kg body weight of Con A diluted in phosphate buffered saline (PBS). The prepared ASCs (1.0×10^6 cells/ 195 μ L PBS) were mixed with 5 μ L Novo-Heparin (10,000 Units/10 mL, Mochida Pharmaceutical, Tokyo, Japan), and then transplanted into mice via a tail vein at 30 min after Con A-administration. As the control group (without ASC transfer), 200 μ L of PBS was injected into Con A-administered mice at the same time point (Fig. 4A). Seven to eight mice were used for each treatment group.

3.2.3 Measurement of liver enzymes

Mice were anesthetized by diethyl ether and the whole blood was collected at 8 and 24 h after Con A administration. Blood samples were allowed to clot for 30 min at room temperature and centrifuged at 15,000 rpm for 3 min, and then the sera were collected. Alanine aminotransferase (ALT) in the serum was measured by the BBx system (Nittobo Medical Co., Ltd, Tokyo, Japan).

3.2.4 qRT-PCR analysis for cytokines, chemokines and cell surface markers

The quantitative real-time reverse-transcription polymerase chain reaction (qRT-PCR) was performed using total RNA prepared from liver tissue with an RNeasy minikit (Qiagen, Tokyo, Japan). The RNA was subjected for first-strand cDNA synthesis using PrimeScript RT Master Mix (Takara Bio Inc, Shiga, Japan) according to the manufacturer's instructions. Then, qRT-PCR was performed with ABI PRISM 7000 sequence detection system (Applied Biosystems Japan Ltd, Tokyo, Japan) using SYBR Premix DimerEraser (Takara Bio) according to the manufacturer's instructions. The PCR amplification was performed as follows; an initial denaturing step, 95 °C for 30 s; followed by 45 cycles of 95 °C for 5 s, 55 °C for 30 s, and 72 °C for 31 s. Cytokines and chemokine analyzed were as follows; interleukin (IL)-1 α , IL-4, IL-6, IL-10, interferon (IFN)- γ , tumor necrosis factor(TNF)- α , transforming growth factor (TGF)- β , C-X-C motif chemokine 12 (CXCL12)/stromal cell-derived factor (SDF)-1, inducible nitric oxide synthase (iNOS), indoleamine 2, 3-dioxygenase (IDO)1, CD3 γ , CD4, CD8, CD11b and CD11c. Glyceraldehyde 3-phosphate dehydrogenase (GAPDH) was used as an internal control. All the primers were synthesized by Takara Bio Inc (Table 1 in Chapter 2).

3.3 Results and discussion

3.3.1 Effects of transplanted ASCs on Con A-induced liver injury

In order to evaluate the effects of transplanted ASCs on liver injury induced by Con A, the levels of serum ALT in mice were evaluated at 8 h and 24 h after Con A administration. The ALT levels at 8 h after Con A administration (Con A group) were markedly elevated ($12,617 \pm 3,431$ U/L), however those in ASC-transplanted group (Con A + ASCs group) at the same time point were significantly decreased ($2,633 \pm 578$ U/L). The ALT levels in Con A + ASCs group at 24 h after Con A administration were elevated ($10,617 \pm 4,684$ U/L) compared to those at 8 h,

however still lower than those of Con A group at the same time point ($13,017 \pm 3,563$ U/L) (Fig. 4B).

Moreover, histological changes of the liver at 24 h after Con A administration were observed microscopically, and the degree of liver damage was compared between Con A group and Con A + ASCs group. The necrotic areas with hepatocytes showing acidophilic cytoplasm and condensed nuclei were widely observed in Con A group, while those areas were relatively small in Con A + ASCs group (Fig. 4C). These changes in ALT levels and liver histology by ASC transplantation suggest that ASC transplantation is useful for the treatment of FHF initiated by excessive immune responses.

3.3.2 Cytokines and cell surface lineage markers expressed in the Injured Liver

To elucidate the mechanism of action of ASCs for ameliorating liver injury, hepatic mRNA expression of various cytokines and cell lineage markers were evaluated with qRT-PCR by using liver samples obtained at 24 h after Con A administration. The mRNA expressions such as IL-6, IL-10, IFN- γ and TNF- α related to inflammation were down-regulated in the Con A + ASCs group compared with Con A group. In addition, the expression of TGF- β which may act on suppressing the inflammatory reaction and cell proliferation, was up-regulated in Con A + ASCs group compared with the Con A group (Fig. 5).

In addition, cell lineage markers such as CD3 γ , CD4, CD8 α , CD11b and CD11c were significantly down-regulated in Con A + ASCs group compared with Con A group. These data suggest that the actions of ASCs for ameliorating FHF induced by excessive immune responses are mediated by suppressing inflammatory reactions and by suppressing invasion or proliferation of inflammatory cells including T cells in the liver (Fig. 6).

3.4 Conclusion

The Con A-induced liver injury model in mice is a well-characterized, representative model of acute liver injury; it is caused by excess immune responses and recognized as a model for autoimmune hepatitis in humans⁴⁹. Therefore, I investigated the anti-inflammatory effects of transplanted ASCs using the Con A-induced liver injury model. Previous reports have shown that Con A-induced liver injury was mainly caused by the activation of NKT cells and T cells which produce TNF- α and IFN- γ ⁶⁰.

In this study, the transplantation of ASCs induced the reduction of ALT levels at 8 h and 24 h after Con A injection, and narrowed the area of massive necrosis at 24 h after Con A injection. However, there were no significant differences in the serum ALT levels at 24 h after Con A injection between with and without ASC transplantation. In the early stage of Con A-induced hepatitis mouse model, the liver injury is triggered by activated T cells and NKT cells which produced TNF- α and IFN- γ ⁶⁰. In a later stage, thrombotic microangiopathy caused by the tissue factor (TF)-activated coagulation system is the main mechanism of liver damage⁵⁴. Thus, I suppose that ASCs exerted the immunosuppressive effects by inhibiting the proliferation of immune cells as indicated in the in vitro study and reducing the production of inflammatory cytokines in the early stage, whereas ASCs could not contribute to the improvement of the liver injury in the latter stage. The down-regulation of cell surface markers expressed in the live MSCs induced by Con A may support this hypothesis. There is another report by Kubo *et al.* that describes the effect of ASCs on Con A-induced liver injury model⁵². The effect of ASCs to ameliorate liver injury is more profound in their report than in our current study, however, the results are mostly consistent with each other. I think that our study confirmed their results and successfully appended theoretical bases of ASC therapy for intractable inflammatory diseases.

I herein investigated the immunomodulatory effects of ASCs on FHF with excessive immune responses. The proliferation of LMCs was found to be efficiently inhibited in a dose-dependent manner of ASCs with direct interaction in the cases of PMA plus ionomycin- (T and B cells activation), and Con A-stimulation (T cell activation). Moreover the therapeutic effects of transplanted ASCs on Con A-induced liver injury was confirmed by the reduction of ALT levels, the improvement of liver histology, and the reduction of mRNA expression of cytokines (IL-6, IL-10, IFN- γ and TNF- α) and cell surface lineage markers (CD3 γ , CD4, CD8 α , CD11b and CD11c). Our findings suggest that ASCs exert strong immunomodulatory abilities both in vitro and in vivo and can be a good candidate for the source of cell therapies of FHF.

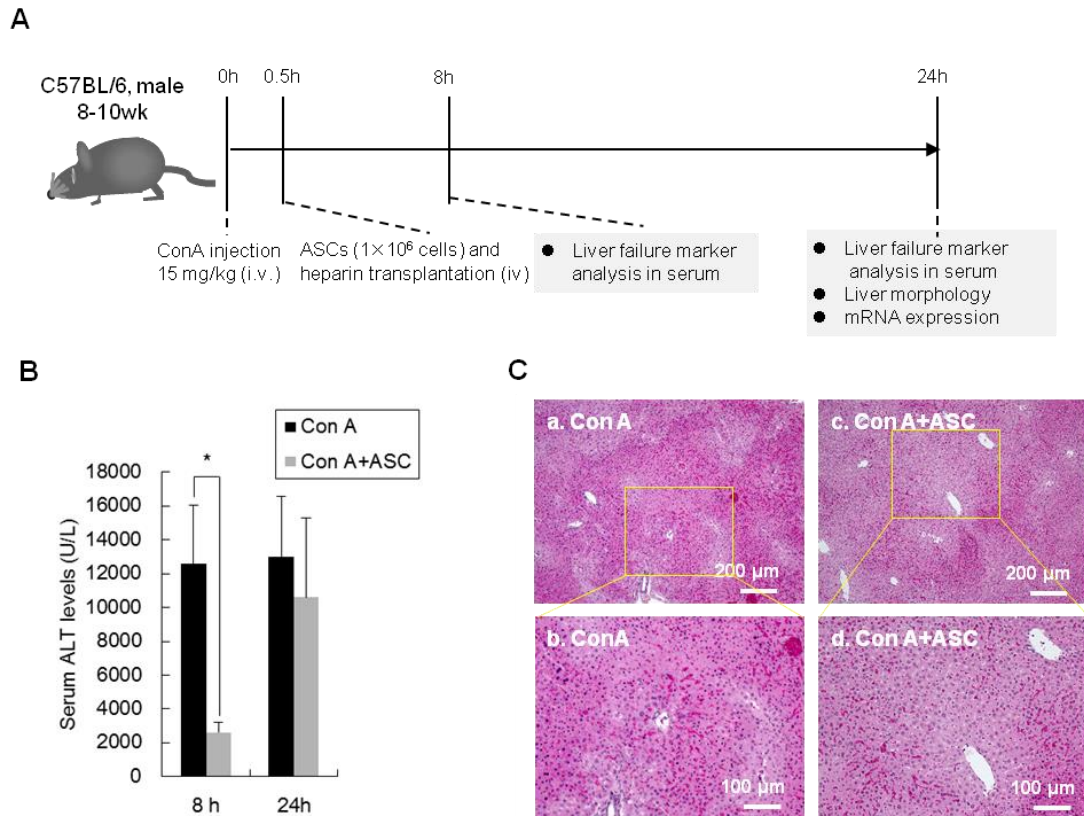


Fig. 4. Effect of ASC transplantation on Con A-induced liver injury in mice

A: The scheme of the in vivo experiment of murine liver injury model. Mice were injected with Con A to induce acute liver failure. After 0.5 h, the transplantation of ASCs was performed. Sera were collected at 8 and 24 h after Con A administration. At 24 h after Con A administration, mice were sacrificed and liver tissue specimens were resected for histological and mRNA expression analysis. **B:** The level of serum alanine aminotransferase (ALT) in Con A-induced mice with or without ASC transplantation. Sera were harvested at 8 and 24 h after Con A-injection ($n = 6$). The data are shown as the means \pm SD values (*; $p < 0.05$). **C:** Hematoxylin and eosin (HE) staining of histological sections of the livers in mice with the treatment of Con A (a,b), Con A+ASCs (c,d). Scale bars indicate 200 μ m (a, c), 100 μ m (b, d), respectively. Representative images are presented ($n = 3$).

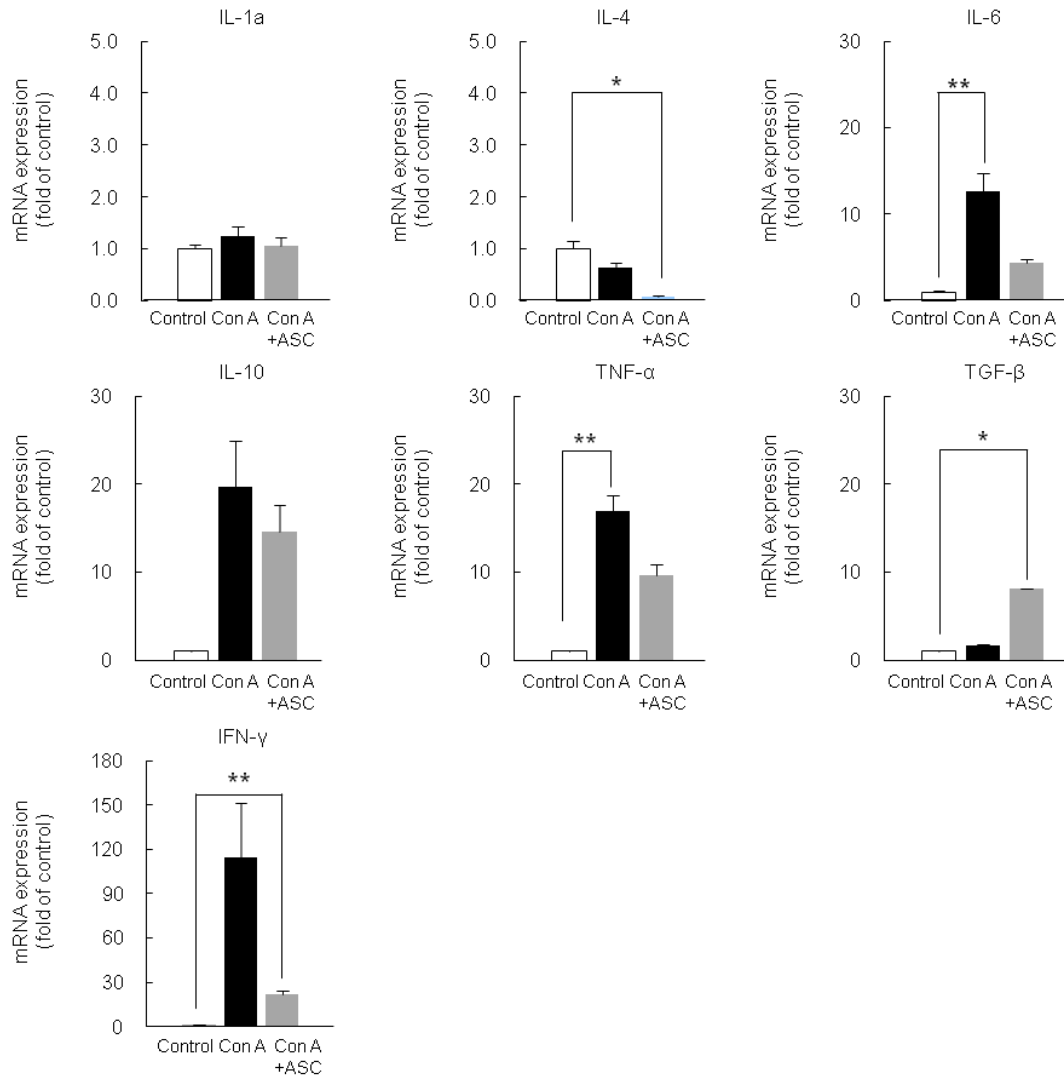


Fig. 5. mRNA expression of cytokines in Con A-induced mice liver after ASC transplantation

mRNA levels of cytokines of liver in Con A-induced mice after ASCs transplantation. The liver samples were harvested at 24 h after Con A administration. Three samples of each group were analyzed and compared with the control (n = 3). The data are shown as the means \pm SE values (*; $p < 0.05$, **; $p < 0.001$).

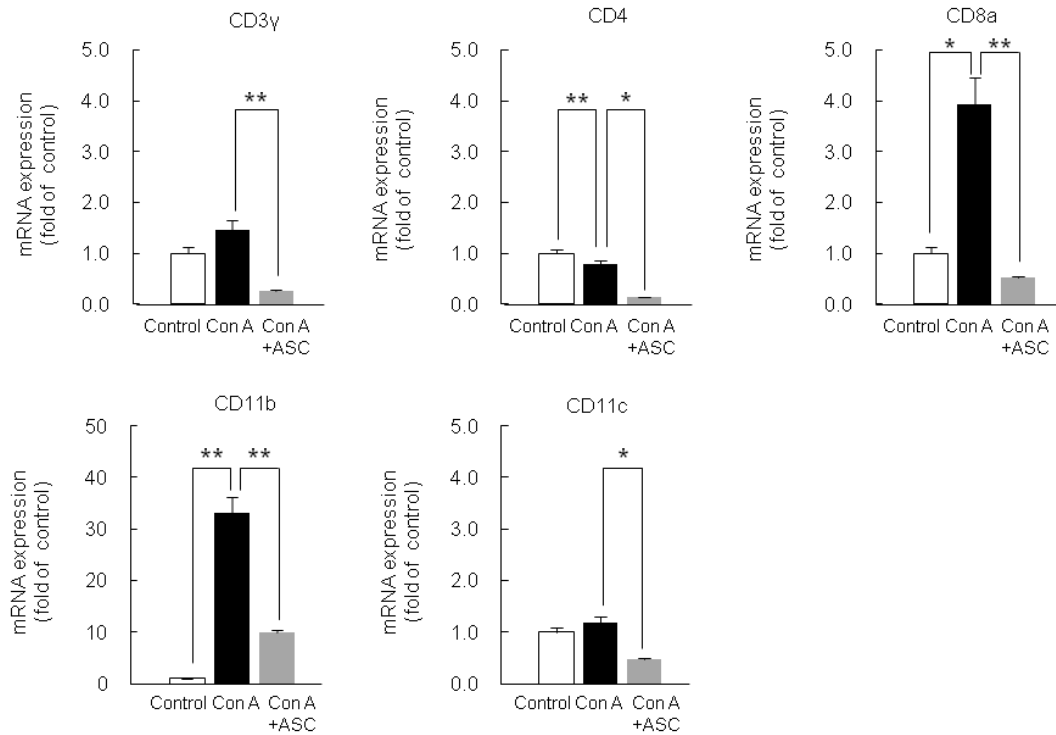


Fig. 6. mRNA expression of cell lineage markers in Con A-induced mice liver after ASC transplantation

mRNA levels of cell lineage markers of liver in Con A-induced mice after ASC transplantation. The liver samples were harvested at 24 h after Con A administration. Three samples of each groups were analyzed and compared with the control (n = 3). The data are shown at the means \pm SE values (*; $p < 0.05$, **; $p < 0.001$).

Chapter 4 Transduction of octa-arginine (R8)- ZnS-ZAIS-COOH (ZZC) into ASCs

4.1 Introduction

Stem cell therapy plays an alternative method of tissue and organ transplantation. I showed the therapeutic effect of adipose-derived stem cells (ASCs) to fulminant hepatic failure (FHF) in Chapter 3. However the behavior and positional information of ASCs were unclear after injection. The development of technologies to label and image ASCs has therefore become important in making further progress in their clinical applications.

Recently, the use of quantum dots (QDs) as inorganic fluorescence probes for biomolecules and live cells is gaining more interest because of high luminance, superior photostability, high quantum yields and wide excitation wavelengths in comparison to organic or protein probes. However, clinical use of QDs is limited by potential toxicity of QDs¹⁸. Most QDs contain toxic elements, including (but not limited to) Cd, Pb, Hg, Se and Te. For advancement of *in vivo* imaging technology, the development of novel QDs with extremely low cytotoxicity (especially Cd-free alternatives) is necessary. The facile synthesis of ZnS-AgInS₂ (ZAIS) as cadmium-free QDs and their application, mainly in solar cells, has been reported by Torimoto *et al.*^{22,23}. In the present study, I investigated the safety and the usefulness for labeling and *in vivo* imaging of a newly synthesized aqueous ZnS-coated ZAIS (ZnS-ZAIS) carboxylated nanoparticles (ZZC) to stem cells. octa-arginine (R8) is highly cationic and can facilitate electrostatic interaction with the plasma membrane and facilitate membrane translocation. The complex of ZZC and octa-arginine (R8) peptides (R8-ZZC) can achieve the highly efficient labeling of adipose tissue-derived stem cells (ASCs). In this chapter, I show the property and transduction efficiency of R8-ZZC.

4.2 Materials and methods

4.2.1 The synthesis of ZnS-coated ZAIS (ZnS-ZAIS) nanoparticles

Oleylamine-covered ZAIS nanoparticles were prepared according to the procedure paper with a slight modification²². Ag(S₂CNEt₂) (13.6 mg), In(S₂CNEt₂)₃ (29.7 mg), and Zn(S₂CNEt₂)₂ (6.8 mg) were dispersed in oleylamine (3.0 mL) and the reaction solution was heated to 180 °C for 30 min under an N₂ atmosphere. The resulting suspension was centrifuged at 4000 rpm for 5 min to remove large particles. ZAIS

nanoparticles were separated from the supernatant with the addition of methanol, followed by centrifugation for 5 min at 4000 rpm.

ZnS-ZAIS nanoparticles were prepared according to a previously published procedure²³. ZAIS nanoparticles, which were prepared as described above, zinc acetate dihydrate (11.8 mg), and thioacetamide (4.0 mg) were dissolved in oleylamine (2.0 mL) and the reaction solution was heat-treated at 180 °C for 30 min under an N₂ atmosphere. After filtration through a syringe filter, the nanoparticles that were obtained were separated from the solution by the addition of methanol, followed by centrifugation for 5 min at 4000 rpm.

ZZC was prepared by a procedure similar to that described paper²⁹. ZnS-ZAIS nanoparticles, which were prepared above, were dissolved in chloroform (1.0 mL). Methanol (1.0 mL) solution containing sodium 3-mercaptopropionic acid (MPA) (100 µL) and tetramethylammonium hydride 25% methanol solution (730 µL) was mixed with the ZnS-ZAIS nanoparticle solution, and the reaction solution was heated to 70 °C for approximately 4 h under an N₂ atmosphere. After the solvent was removed under reduced pressure, the crude product was dissolved in methanol. Chloroform was then added to precipitate ZZC. Finally, centrifugation was performed for 5 min at 4000 rpm. This purification process was repeated several times to remove residual reagents. The resulting precipitate was dried under a vacuum and dissolved in MilliQ water.

4.2.2 The particle properties analysis

The particle size distribution and the zeta potential of ZZC and the R8-ZZC complex (R8-ZZC) in water were measured using a dynamic light-scattering spectrophotometer (ZETASIZER Nano-ZS, Malvern Instruments Limited Japan, Hyogo, Japan). The particle size is shown by the peak of the size distribution graph in Fig.7B,C.

The absorbance spectra of ZZC and R8-ZZC were measured using an 8453A UV-visible spectrophotometer (Agilent Technology, Santa Clara, CA, U.S.A.). The fluorescence spectra were measured using a photonic multichannel analyzer (PMA-12; Hamamatsu Photonics, Shizuoka, Japan). The excitation wavelength was 365 nm. Transmission electron microscopy (TEM, H-7650, Hitachi, Japan) was used to visualize the ZZC and R8-ZZC nanoparticles at an accelerating voltage of 100 kV.

R8-ZZC (ZZC:250 nM, R8:250 μ M) in PBS or transduction medium (DMEM/F12 containing 2% FBS and 100 U/mL penicillin/streptomycin) was incubated for various length of time (0, 1, 3, 5 and 7 days) at 37°C. The phase and fluorescence images were observed by 8 mega pixel digital camera and the intensities were measured using an IVIS Lumina K Series III (PerkinElmer, Inc., Massachusetts, USA).

4.2.3 The transduction of R8-ZZC into ASCs

ZZC (250 nM) and R8 were mixed for 15 min at room temperature in various ratios (ZZC:R8 = 1:0, 1:10, 1:100, 1:1000) in order to determine the optimal concentration ratio of ZZC/R8 for inducing transduction into ASCs. ASCs were incubated with R8-ZZC in a transduction medium at 37°C. After 4 h incubation, the cells were washed using transduction medium. The transduction of ZZC into ASCs was observed by phase-contrast fluorescence microscopy and high-speed multiphoton confocal laser microscopy (A1MP⁺/A1RMP⁺, Nikon, Tokyo, Japan). The transduction efficiency was evaluated by flow cytometry (BD LSRFortessa™ X-20, Japan BD, Tokyo, Japan).

4.3 Results and discussion

4.3.1 The properties of ZZC and R8-ZZC

TEM and fluorescence images and the particle size distribution, the zeta potential, absorbance and the fluorescence spectra of ZZC and R8-ZZC are shown in Fig. 7B and C. The ZZC and R8-ZZC particles were observed to be smaller than 10 nm in size (Fig. 7B-a and 7C-a). The particle sizes of ZZC and R8-ZZC were 5.1 nm and 9.1 nm, respectively, and the zeta potentials were -11.0 mV and +15.3 mV (Fig. 7B-b and 7C-b). Orange and red fluorescence derived from ZZC and R8-ZZC, respectively could be observed in a water (Fig. 7B-c and 7C-c). The fluorescence maximum wavelengths of ZZC and R8-ZZC were 657 nm and 690 nm, respectively (Fig. 7B-d and 7C-d).

4.3.2 The fluorescence stability of R8-ZZC in cell culture medium

To investigate the fluorescence stability of R8-ZZC, the fluorescence images of R8-ZZC in PBS or cell culture medium under day light and UV light were observed. The red fluorescence derived from R8-ZZC could be detected for at least 7 days in PBS

and cell culture medium (Fig. 7D-a). In addition, the fluorescence intensity of R8-ZZC in the cell culture medium was lower than that in PBS, however the fluorescence intensities of R8-ZZC (8 nM of ZZC) were maintained in PBS and cell culture medium (Fig. 7D-b). These data suggest that R8-ZZC can be used for cell labeling in cell culture medium.

4.3.3 The optimal concentration ratio of ZZC and R8

To investigate the optimal concentration ratio of ZZC and R8 for the labeling of ASCs, 250 nM of ZZC was mixed with various concentrations of R8 (0, 2.5, 25 and 250 μ M), and these complexes were transduced into ASCs for 12 h. The red fluorescence of ZZC-labeled ASCs could be detected when the R8 concentration of more than 25 μ M were used (Fig. 8A-a-h). The labeling efficiency and fluorescence intensity of R8-ZZC for ASCs were 78.0% and 7290 (25 μ M R8), and 96.5% and 7973 (250 μ M R8), respectively (Fig. 8A-i-l, B-a,b).

In addition, to decide the optimal transduction time of R8-ZZC to ASCs, R8-ZZC (ZZC:R8 = 1:1000) was transduced into ASCs for 1, 4 and 12 h, and then the labeling efficiency and intensity were assessed. The labeling efficiency and the fluorescence intensity were 95.8% and 4235 (1 h); 96.2% and 6006 (4 h); and 96.5 % and 7973 (12 h), respectively. Notably, more than 95% of the ASCs could be labeled within 1 h. (Fig. 8C). The transduction of ZZC using R8 into ASCs was also observed as red fluorescence derived from ZZC by high-speed multiphoton confocal laser microscopy (Fig. 8D). These data suggest that the optimal concentration ratio of ZZC to R8 is 1:1000, and that almost all ASCs could be labeled with R8-ZZC by at least 1 h of transduction.

4.4 Conclusion

I described the successful synthesis of water soluble ZnS-ZAIS with carboxyl group (ZZC) nanoparticles that show fluorescence at approximately 650 nm, almost all of the particles were smaller than 10 nm and were negatively charged. ZZC could show the strong fluorescence (657 nm) in water solution. On the other hand, R8-ZZC was positively charged due to the presence of R8 molecules which is a cell-penetrating peptide, and could show strong red fluorescence in water solution. R8-ZZC maintained its strong fluorescence (690 nm) in PBS or cell culture medium for at least a week. R8-ZZC was therefore suitable for cell labeling in cell culture medium.

The optimal complex ratio of ZZC and R8 molecules for ASCs labeling was 1:1,000. Yukawa *et al.* have already revealed that the optimal complex ratio CdSe-based QDs (Invitrogen; Qdot ITK Carboxyl Quantum Dots) and R8 molecules is 1:10,000,¹⁷ thus it required one-tenth the number of R8 molecules that were needed for ZZC. It is thought that this is due to the size of the nanoparticles and the amount of carboxyl group on the surface. On the other hand, the labeling time was not changed, and almost all of the ASCs could be labeled with R8-ZZC within 1 h. Cell-penetrating peptides, including R8 molecules, are reported to be introduced into cells via macropinocytosis in the endocytosis pathway^{61,62}. Thus R8-ZZC is also thought to be introduced into ASCs by macropinocytosis. R8-ZZC is therefore expected to have the potential to quickly label many types of cells, including stem cells.

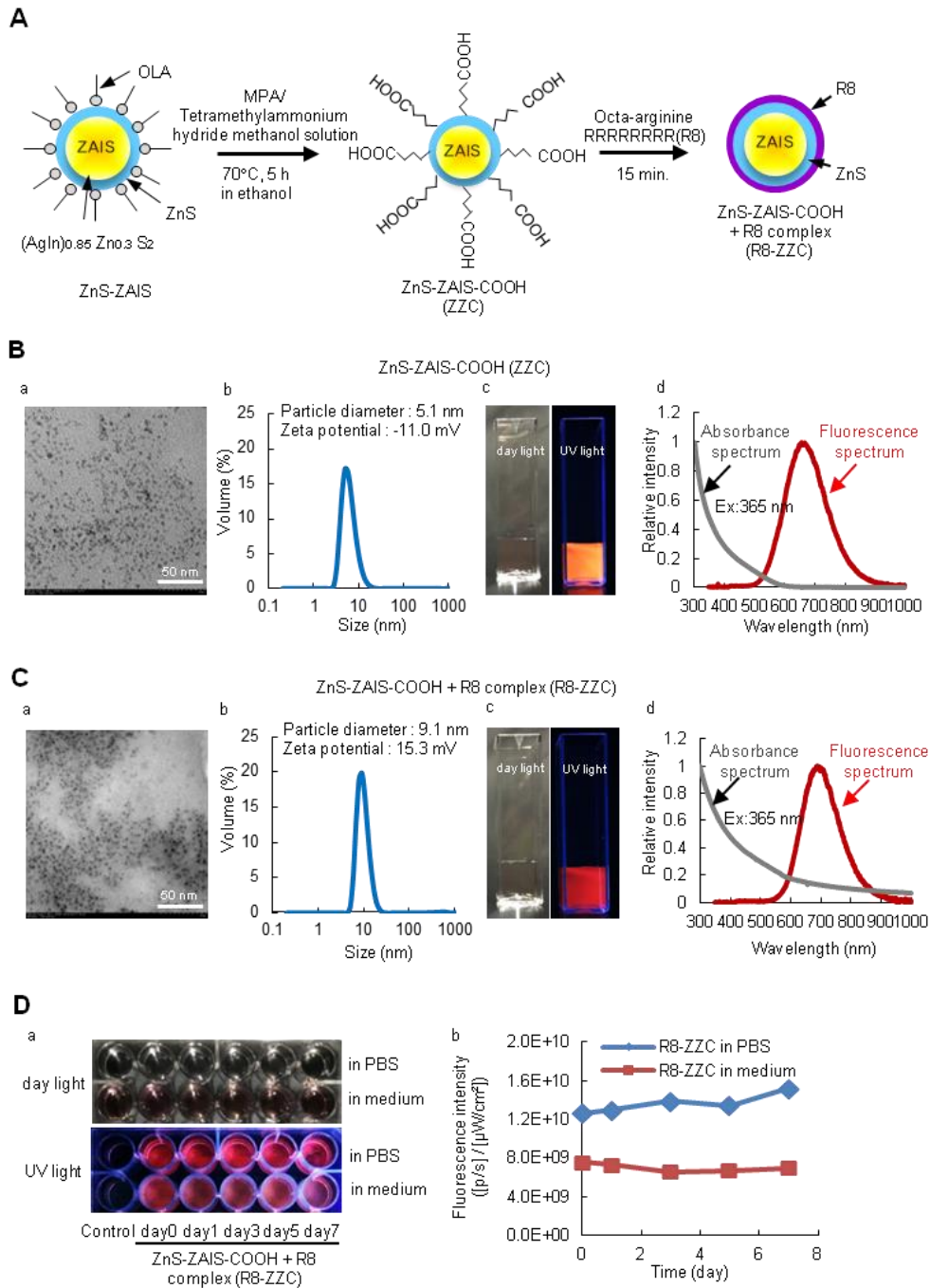


Fig. 7. The synthesis protocol and the fluorescence properties of ZcC and R8-ZcC

A: A schematic diagram of the synthesis of ZcC and R8-ZcC. B: An TEM image (a), the particle diameter and zeta potential (b), fluorescence images (excited by day light and UV light) (c), and the absorbance and fluorescence spectrum (d) of ZcC in water. C: An SEM image (a), the particle diameter and zeta potential (b), fluorescence images (excited by day light and UV light) (c), and the absorbance and fluorescence spectrum (d) of R8-ZcC in water. D: The fluorescence images (a) and intensities (b)

of R8-ZZC (8 nM of ZZC) in PBS or the culture medium of ASCs after 7 days of culturing (37°C, 5% CO₂).

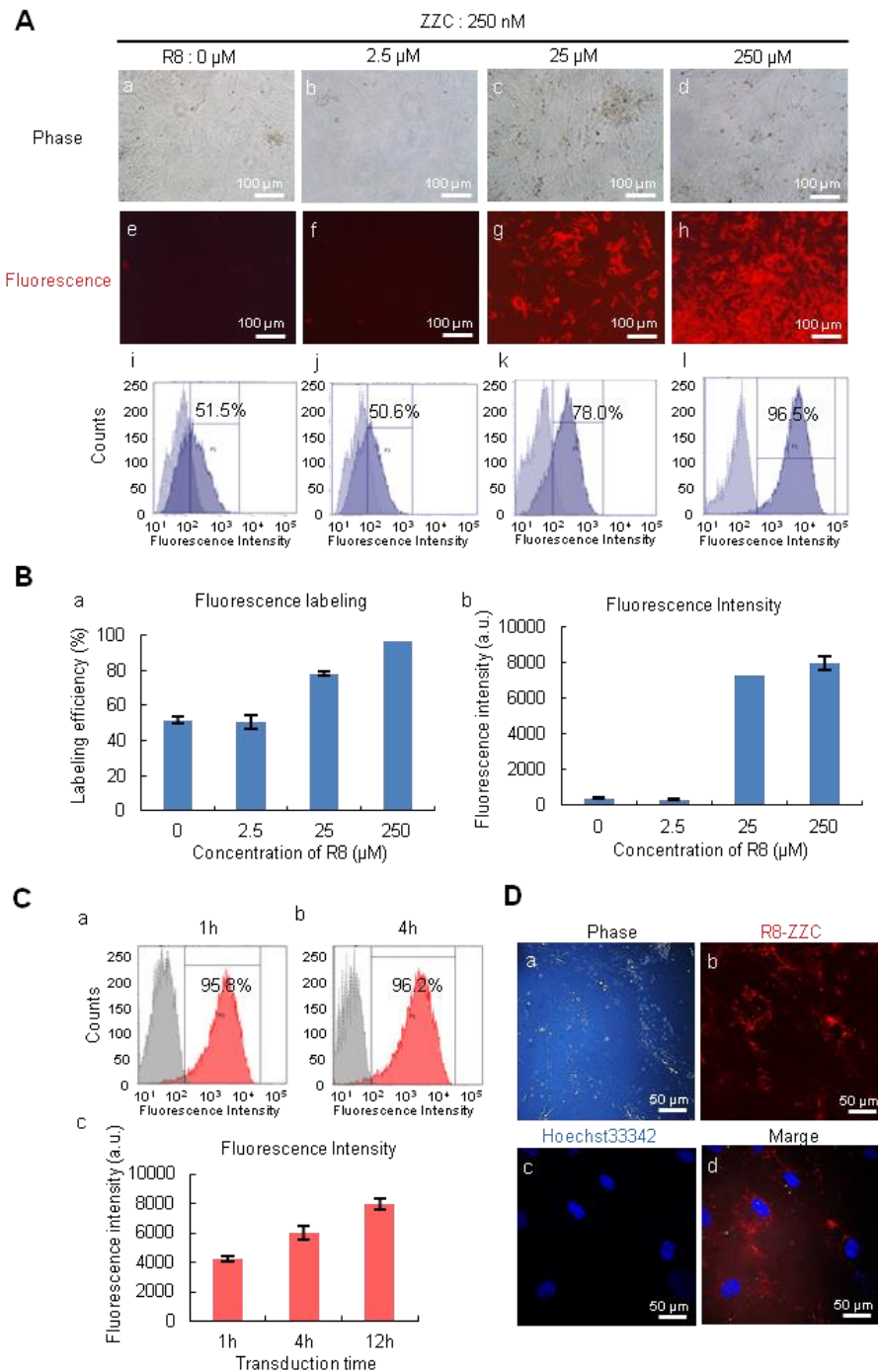


Fig. 8. The optimal concentration ratio of ZZC and R8 for labeling ASCs

A: The phase (a-d) and fluorescence (e-h) images of ASCs labeled with ZZC (250 nM) and various concentrations (0, 2.5, 25, 250 μ M) of R8 complexes. A flow cytometry analysis of the labeling efficiency and fluorescence intensity (i-l). B: Graphs of the labeling efficiency (a) and fluorescence intensity (b) of ASCs labeled

with ZZC (250 nM) and various concentrations (0, 2.5, 25, 250 μ M) of R8 complexes as determined flow cytometry. C: A flow cytometry analysis of the labeling efficiency and fluorescence intensity (a-c) of ASCs labeled with the optimal concentration ratio of ZZC (250 nM) and R8 (250 μ M) under various transduction times. D: Confocal microscopy images of R8-ZZC-labeled ASCs (phase contrast of ASCs (a), the red fluorescence of ZZC (b), the blue fluorescence of a nucleus stained with Hoechst33342 (c), and a merged image (d)).

Chapter 5 The evaluation R8-ZZC labeled ASCs

5.1 Introduction

The fluorescence labeling of ASCs by ZZC and R8 complex (R8-ZZC) was addressed in Chapter 4. It suggests that R8-ZZC is maintained its strong and stably fluorescence in PBS or cell culture medium, and is expected to have the potential to quickly label many types of cells. However, cytotoxic affect of ZZC to ASCs was unclear. For their clinical applications, the development of novel QDs with extremely low cytotoxicity (especially Cd-free alternatives) is necessary. In this chapter, I show that the influence of R8-ZZC labeling on the properties of ASC, especially in regard to the induction of major inflammatory cytokines, was investigated

5.2 Materials and methods

5.2.1 The cytotoxicity test of R8-ZZC to ASCs

ASCs (1×10^4 cells) were seeded in a 96-well plate (BD Falcon; BD Biosciences,) with 100 μ L of culture medium, and the cells were cultured for 24 h. ZZC (0-400 nM) and R8 were mixed at the optimal ratio of 1: 1,000, and R8-ZZC nanoparticles were transduced into ASCs in a transduction medium. After 4 h transduction, the ASCs were washed twice with a transduction medium, and were incubated for 24 h. The viable cells were then counted using a cell counting kit-8 (CCK-8). CCK-8 reagent (10 μ L) was added to each well and the reaction was allowed to proceed for 2 h. The absorbance of the sample at 450 nm was measured against a background control using a microplate reader (POLARstar OPTIMA; BMG LABTECH, Ortenberg, Germany).

5.2.2 The proliferation of R8-ZZC labeled ASCs

ASCs (4×10^3 cells) were seeded in a 96-well plate with 100 μ L of culture medium for 1 day and then transduced with ZZC using R8 at various concentrations for 4 h. ZZC (0, 62.5, 125, 250 nM) and R8 were mixed at the optimal ratio of 1:1000, and then each complex was transduced into ASCs. The cells were the washed and the medium was replaced with 100 μ L of new culture medium. After 2 and 4 days, the viable cells were counted using a CCK-8. The method was the same as that which was used to determine cytotoxicity.

5.2.3 Adipogenic and osteogenic differentiation

Adipogenic differentiation was induced by culturing the cells for 3 days in DMEM (high glucose) containing 100 mM indometacin, 1 mM dexamethasone, 1 mM hydrocortisone, 10 mM insulin (Sigma, I-5500) and 10% FBS. The cells were then further cultured in DMEM (high glucose) containing 10% FBS for 2 weeks and the medium was changed every 3 days. Differentiation was confirmed by the conventional microscopic observation of intracellular lipid droplets. Oil Red O staining was used as an indicator of intracellular lipid accumulation.

Osteogenic differentiation was induced by culturing the cells for 2 weeks in DMEM containing 200 nM dexamethasone, 50 mM ascorbate-2-phosphate (Wako Pure Chemical Industries Ltd., 013-12061), 10 mM α -glycerophosphate (Sigma, G-9891) and 10% FBS. The differentiation was confirmed by the staining of any alkaline phosphatase activity.

5.2.4 The measurement of inflammation markers

ASCs (1×10^5 cells) were seeded into a 24-well plate and cultured for 24 h. ZZC (0, 25, 125, 250 nM) and R8 were mixed at the optimal ratio of 1:1000, and each complex was transduced into ASCs. After 4 h incubation, the ASCs were replaced with new cell culture medium and were cultured for 1 or 3 days. The cell culture medium was collected and the levels of five types of cytokines (TNF- α , IFN- γ , IL-12p70, IL-6 and MCP-1) were measured by using Cytometric Bead Array Mouse Inflammation Kit (BD Bioscience, 552364).

5.3 Results and discussion

5.3.1 The cytotoxicity of R8-ZZC to ASCs

To examine the cytotoxicity of R8-ZZC to ASCs, various concentrations (0, 62.5, 125, 250 and 400 nM) of ZZC were transduced into ASCs using R8 for 4 h at the optimal ratio, and the ASCs were incubated for 24 h. More than 95% of the ASCs were confirmed to be alive in the ZZC concentration of less than or equal to 250 nM. Significant cytotoxicity was observed in the ASCs transduced with 400 nM of ZZC, however, more than 80% of the cells remained alive (Fig. 9A-a).

The influence R8-ZZC on the proliferation rate of ASCs was also examined within the non-cytotoxic range of concentrations. ASCs were confirmed to exhibit a growth rate that was nearly equal to normal ASCs. There were no significant

differences in these concentrations (Fig. 9A-b). These data suggest that ASCs can be labeled in a ZZC concentration of less than or equal to 250 nM using R8.

5.3.2 The inflammatory cytokine production of R8-ZZC-labeled ASCs

To investigate whether R8-ZZC labeling causes an inflammation reaction in ASCs, the levels of major inflammatory cytokines were measured in the culture supernatant of R8-ZZC-labeled ASCs (250 nM of ZZC) after 1 or 3 days of culturing and the production level was compared with that in non-labeled ASCs. No significant differences were observed between the non-labeled and labeled ASCs in the levels of the major inflammation cytokines (TNF- α , IFN- γ , IL-12p70, IL-6 and MCP-1). The level of IL-12p70 tended to be higher in R8-ZZC-labeled ASCs in comparison to non-labeled ASCs, however, the differences was not statistically significant. No significant differences were observed in the levels of the other cytokines. In addition, concentration-dependent changes were observed with different concentrations of R8-ZZC (Fig. 9B). These data suggest that ZZC does not influence the inflammation of ASCs.

5.3.3 The differentiation of R8-ZZC-labeled ASCs

To examine the influence of R8-ZZC (250 nM of ZZC) on the differentiation capacity of ASCs, normal (non-labeled) and labeled ASCs transduced with R8-ZZC were differentiated into adipocytes and osteoblasts. The differentiations of R8-ZZC-labeled ASCs into both adipocytes and osteoblasts was similar to that observed in normal ASCs (Fig. 9C). These data suggest that R8-ZZC (250 nM of ZZC) does not affect the differentiation of ASCs.

5.4 Conclusion

The cytotoxicity of CdSe-based QDs (Invitrogen; Qdot ITK Carboxyl Quantum Dots) to ASCs was revealed greater than or equal to that observed in QDs at a concentration of 16 nM,¹⁷ however, R8-ZZC was confirmed to have no cytotoxic effects in ASCs at ZZC concentrations less than or equal to 250 nM. ZZC does not contain cytotoxic elements (such as Cd and Se), thus the cytotoxicity of R8-ZZC to ASCs appears to be extremely suppressed in comparison to CdSe-based QDs²¹. No influence of R8-ZZC on the self-renewal or the ability to differentiate into adipocytes or osteocytes was confirmed at ZZC concentrations less than or equal to 250 nM.

The influence of R8-ZZC on the production of inflammatory cytokines in ASCs was also examined. Ho *et al.* reported that CdSe-based QDs induced MCP-1 expression via the MyD88-dependent Toll-like receptor signaling pathways in macrophages⁶³. Furthermore, Wang *et al.* assessed the immunotoxicity of CdSe-based QDs in macrophages, lymphocytes and BALB/c mice⁶⁴. However, little is known about the influence of various types of QDs on the production of inflammatory cytokines in ASCs. In the present study, the levels of MCP-1 and IL-6 was found to be increased by labeling with 8 nM of CdSe-based QDs (data not shown). In contrast, R8-ZZC did not induce the production of major inflammatory cytokines. These results may be the first report of the influence of QDs on the inflammatory cytokines in ASCs. Based on the finding of the present study, R8-ZZC is expected to be more useful for stem cell labeling than CdSe-based QDs. In the future, however, further investigations should be performed to elucidate the detailed mechanisms underlying the differences in the cytotoxicity of CdSe-based QDs and ZZC.

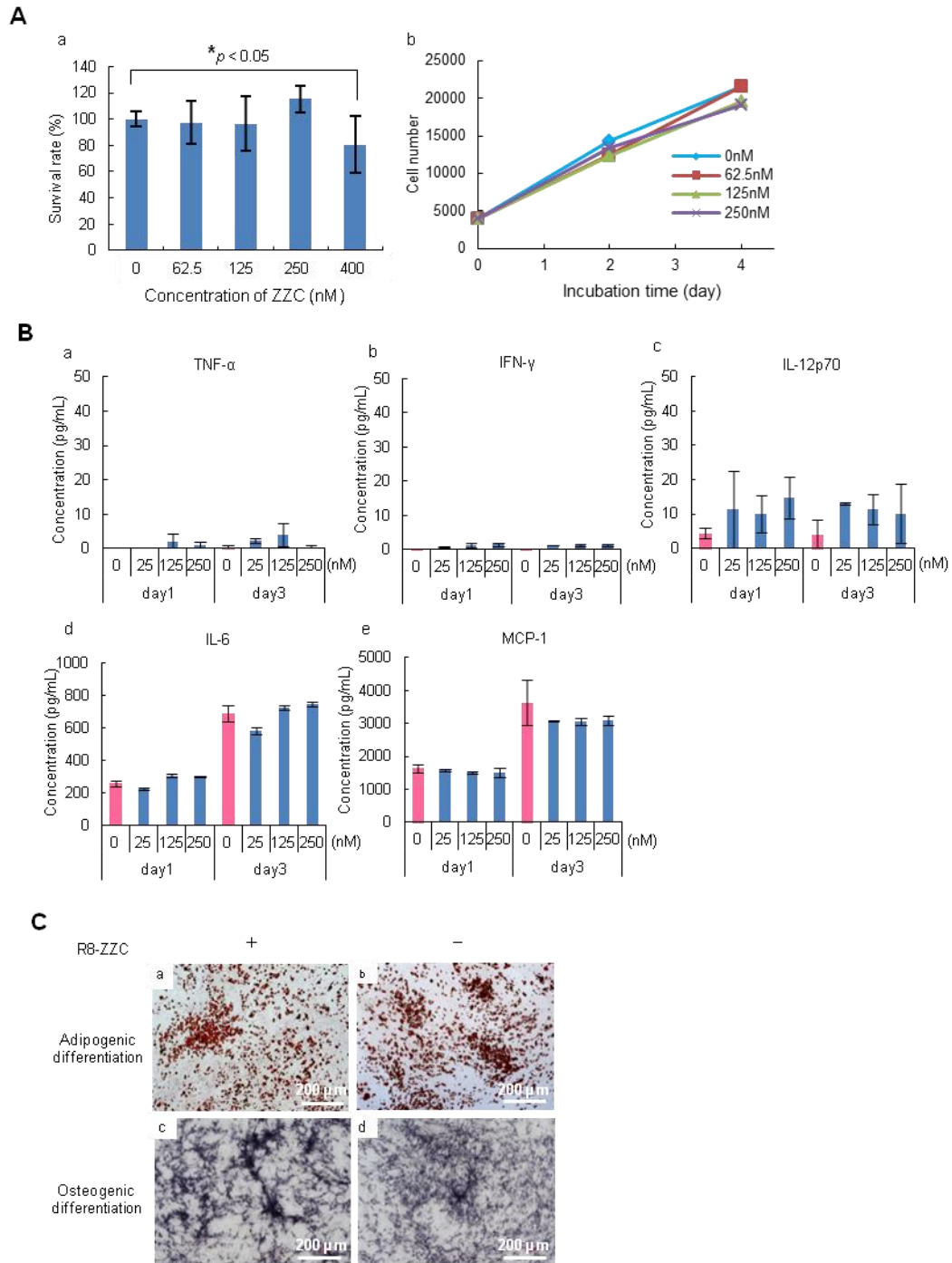


Fig. 9. The influence of R8-ZCC on ASCs

A: The cytotoxicity of R8-ZCC (0, 62.5, 125, 250, 400 nM of ZCC) on ASCs at 24 h incubation after 4 h transduction (a), and the proliferation rate of R8-ZCC-labeled ASCs (0, 62.5, 125, 250 nM of ZCC) after 4 h transduction (b). The data are shown as the mean \pm SD. $*p < 0.05$. B: The major inflammatory cytokine levels (TNF- α , IFN- γ , IL-12p70, IL-6 and MCP-1) of R8-ZCC-labeled ASCs (0, 62.5, 125, 250 nM of ZCC) after 1 or 3 days of incubation. C: The differentiation of R8-ZCC-labeled ASCs (250 nM of ZCC) (a,c) or non-labeled ASCs (b,d) into adipocytes and osteocytes.

Chapter 6 *In vivo* and *ex vivo* imaging of R8-ZZC-labeled ASCs

6.1 Introduction

The safety of newly synthesized form of ZZC was assessed in the previous chapter. The cytotoxicity of R8-ZZC to ASCs was found to be extremely low in comparison to CdSe-based QDs, and R8-ZZC was not found to influence the proliferation rate or differentiation ability of ASCs.

Fluorescence imaging is expected as *in vivo* imaging by the high resolution that can observe a single cells. It is necessary to see whether the observation of the *in vivo* transplant cell is possible. To examine R8-ZZC resolution into the body, *in vivo* fluorescence imaging of transplanted R8-ZZC-labeled ASCs was performed in mice using an *in vivo* imaging system.

6.2 Materials and methods

6.2.1 The observation of R8-ZZC-labeled ASCs in the mice

ZZC was transduced into ASCs using R8 in the same manner as described above. The fluorescence images and intensities of ASCs (0.31, 0.63, 1.3, 2.5, 5.0, and 10×10^5 cells) labeled with ZZC (250 nM) in 1.5 mL tubes were investigate using an IVIS Lumina K Series III (excitation filter: $500 \text{ nm} \pm 20 \text{ nm}$, emission filter: $790 \text{ nm} \pm 40 \text{ nm}$). Next, the R8-ZZC-labeled ASCs were subcutaneously transplanted with PBS (50 μL) into the backs of C57BL/6 mice. The fluorescence images and intensities were investigated using an IVIS Lumina K Series III with the above-described filter conditions. The correlation coefficient between the number of R8-ZZC-labeled ASCs and the fluorescence intensity was calculated.

For the *in vivo* fluorescence imaging studies, I used mice that were given food which did not include any fluorescence components (alfalfa-free feed) for 1 week in order to reduce the effects of the autogenic fluorescence from the gastrointestinal tract. R8-ZZC-labeled ASCs (1×10^6 cells) were then transplanted with saline (0.15 mL) in combination with heparin through the tail vein. The mice were anesthetized and were monitored from 10 min after transplantation using an IVIS Lumina K Series III (excitation filter: $660 \text{ nm} \pm 20 \text{ nm}$), emission filter: $790 \text{ nm} \pm 40 \text{ nm}$).

6.2.2 The observation of R8-ZZC-labeled ASCs in the organs

For *ex vivo* fluorescence imaging, the major organs (liver, kidneys, lungs, spleen and heart) were harvested and immediately subjected to fluorescence imaging using an IVIS Lumina K Series III with the same conditions that were used for *in vivo* imaging. The region of intensity (ROI) was measured with the assistance of the IVIS Lumina K Series III.

6.2.3 Multiphoton analysis

Mice transplanted with R8-ZZC-labeled ASCs were sacrificed, and then the five major organs (heart, lungs, liver, spleen and kidneys) were extracted. These organs were dipped in PBS (500 μ L) with isolectin conjugated with FITC (5 μ L) for 12 h in order to dye and clear the blood vessels in the organs. The organs were then placed on a 35 ϕ mm glass bottom dish and observed under high-speed multiphoton confocal laser microscopy (A1MP⁺/A1RMP⁺, Nikon, Tokyo, Japan).

6.3 Results and discussion

6.3.1 Relevance of fluorescence intensity to cell numbers

To examine whether R8-ZZC-labeled ASCs (250 nM of ZZC) could be quantitatively detected, various numbers of the labeled ASCs (3.1×10^4 , 6.3×10^4 , 1.3×10^5 , 2.5×10^5 , 5.0×10^5 , 1.0×10^6 cells) were collected in PBS and spun down. The cell pellets were then prepared for a fluorescence analysis in microtubes (Fig. 10A-a). The labeled cell pellets could be quantitatively detected at high levels of fluorescence intensity (Fig. 10A-b,c). These data suggest that the R8-ZZC-labeled cells could be detected when the fluorescence intensity was sufficient for cell visualization by fluorescence imaging.

To assess whether images of transplanted R8-ZZC-labeled ASCs (250 nM of ZZC) could be obtained in mice, various numbers of the labeled ASCs (3.1×10^4 , 6.3×10^4 , 1.3×10^5 , 2.5×10^5 , 5.0×10^5 , 1.0×10^6 cells) were transplanted on the backs of mice (Fig. 4B-a). The transplanted R8-ZZC-labeled ASCs could be detected quantitatively as well as by *in vitro* fluorescence imaging (Fig. 10B-b,c). Moreover, R8-ZZC-labeled ASCs (1.0×10^6 cells) were transplanted through the tail vein of a mouse to examine whether the fluorescence derived from ZZC could be detected and the distribution of the transplanted ASCs could be shown in the major five organs (Fig. 11A-a). When mice were sacrificed at 10 min after transplantation, the

fluorescence derived from ZZC could be detected in the lungs and liver using an IVIS imaging system (Fig. 11A-b).

6.3.2 *Ex vivo* fluorescence imaging of the transplanted R8-ZZC-labeled ASCs

Five organs (liver, kidneys, lungs, spleen and heart), in which almost all of the transplanted ASCs were predicted to accumulate, were isolated from mice transplanted with R8-ZZC-labeled ASCs, and *ex vivo* fluorescence imaging was conducted. The strong fluorescence derived from ZZC was detected from the lungs and liver, little or no fluorescence was detected from the kidneys, spleen and heart. The fluorescence intensity of *ex vivo* fluorescence imaging is closely reflected, the level of ZZC maintained inside each organ, because of the deep penetration of the excitation and the emission light in the NIR region. Consequently, the rates of transplanted ASCs that accumulated in the lungs and liver were approximately 40% and 60%, respectively (Fig. 11A-d).

Moreover, to investigate the accumulation condition in which transplanted R8-ZZC-labeled ASCs in the lungs and liver, isolated lungs and liver in which the vessels showed with green fluorescence due to isolectin staining were observed under high-speed multiphoton confocal laser microscopy. Red fluorescence derived from the transplanted R8-ZZC-labeled ASCs was observed in both the lungs and liver, however the accumulation was in two types of organs (Fig. 11B,C-a,b). ASCs were observed to aggregate with high efficiency in the lungs, whereas almost all of the ASCs isolated and few aggregates were observed in the blood vessels of the liver (Fig. 11B,C-c). These data suggest that ZZC is useful for the *in vivo* visualization of transplanted ASCs.

6.4 Conclusion

R8-ZZC-labeled ASCs in the microtube could be quantitatively detected (depending on the number of ASCs) by analyzing the fluorescence intensity using an *in vivo* fluorescence imaging system. The subcutaneously transplanted R8-ZZC-labeled ASCs on the backs of mice could also be quantitatively detected. In addition, R8-ZZC-labeled ASCs that were intravenously transplanted through the tail vein could be detected, and similarly to previous reports) almost all of the transplanted ASCs were found to accumulate in the lungs and liver. However, the details of the accumulation of transplanted ASCs in the lungs and liver have remained poorly understood. I

therefore investigated the accumulation of transplanted ASCs using high-speed multiphoton confocal laser microscopy and found that the conditions in the lungs were different to those in the liver.

The transplanted ASCs formed aggregates at many sites in the lungs, but not in the liver. The blood vessels in the lungs were observed to be very fine (Fig 11B-c). It was therefore hypothesized that the size of the transplanted ASCs might have caused them to aggregate at the same point in a narrow vein. In contrast, the blood vessels in the liver were not as fine (Fig 11C-c), thus individually ASCs appeared to accumulate over relatively large areas of the liver. However, almost all of the ASCs were found in the blood vessels, and they could not pass the perisinusoidal space. If the transplanted ASCs are maintained in the liver for a long period of time and differentiate into hepatocytes with high efficiency, then a sinusoidal dilator may be useful. This study suggests that ZZC labeling using R8 can be used for the labeling and *in vivo* imaging of ASCs. The findings of the present study are expected to contribute to further progress in their clinical applications.

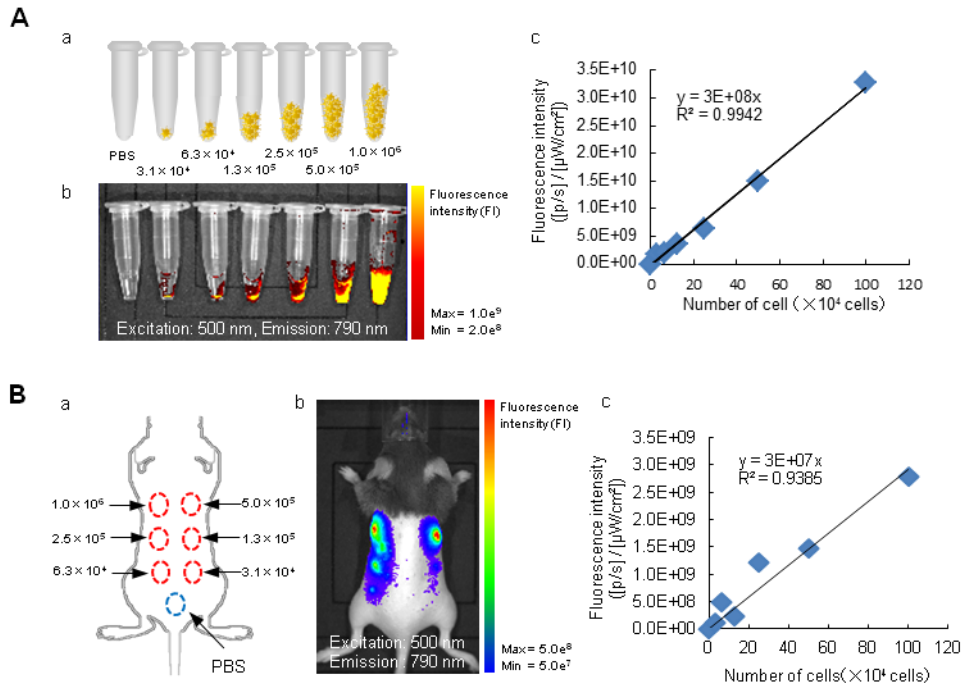


Fig. 10. *In vivo* fluorescence imaging of the mouse R8-ZZC-labeled ASCs after subcutaneous transplantation

A: *In vitro* fluorescence imaging of various numbers of ASCs (3.1×10^4 , 6.3×10^4 , 1.3×10^5 , 2.5×10^5 , 5.0×10^5 , 1.0×10^6 cells) labeled with R8-ZZC (250 nM of ZZC) (a,b). Excitation: 500 nm, Emission: 790 nm. The linear relationship between the number of R8-ZZC-labeled ASCs and the fluorescence intensity ($R^2 = 0.9942$) (c). **B:** *In vivo* fluorescence imaging of ASCs (3.1×10^4 , 6.3×10^4 , 1.3×10^5 , 2.5×10^5 , 5.0×10^5 , 1.0×10^6 cells) labeled with R8-ZZC (250 nM of ZZC) after subcutaneous transplantation onto the back of a mouse (a,b). Excitation: 500 nm, Emission: 790 nm. The linear relationship between the number of R8-ZZC-labeled ASCs and the fluorescence intensity ($R^2 = 0.9385$) (c).

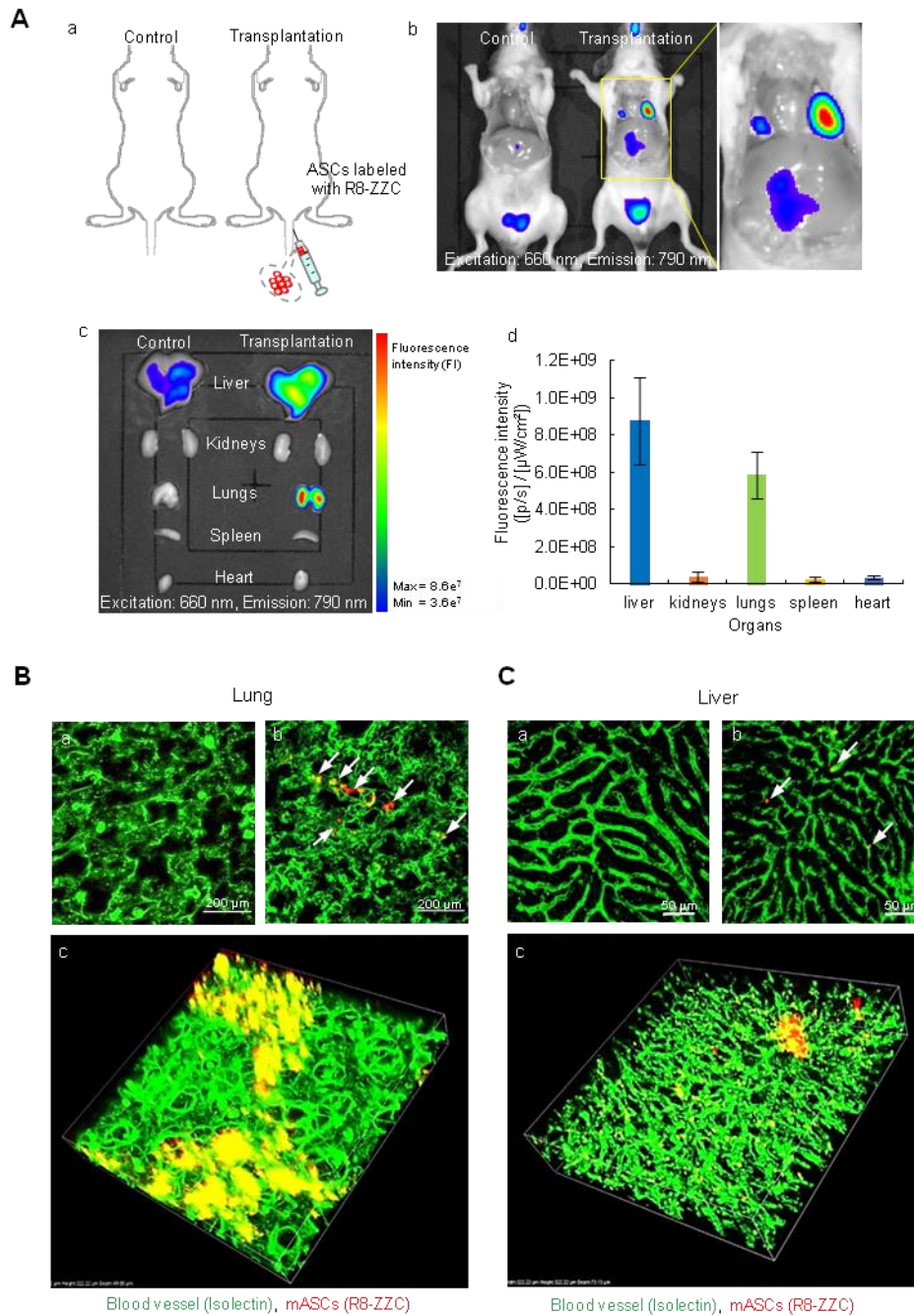


Fig. 11. *In vivo* and *ex vivo* fluorescence imaging of R8-ZZC-labeled ASCs after intravenous transplantation

A: *In vivo* fluorescence imaging of ASCs (1.0×10^6 cells) labeled with R8-ZZC (250 nM of ZZC) after intravenous transplantation (a,b). *Ex vivo* imaging and the fluorescence intensity of five major organs (liver, kidneys, lungs, spleen and heart) eviscerated from a transplanted mouse (c,d). **B:** Multiphoton confocal images of the lung eviscerated from a control mouse (non-transplantation) (a) and a mouse after the transplantation of R8-ZZC-labeled ASCs (250 nM of ZZC) (b). A 3D confocal image of the lung eviscerated from the mouse after transplantation of R8-ZZC-labeled ASCs

(250 nM of ZZC) (c). C: Multiphoton confocal images of the liver eviscerated from a control mouse (non-transplantation) (a) and a mouse after the transplantation of R8-ZZC-labeled ASCs (250 nM of ZZC) (b). A 3D confocal image of the liver from a mouse after the transplantation of R8-ZZC-labeled ASCs (250 nM of ZZC) (c). The blood vessels and ASCs were stained with isolectin (green fluorescence) and ZZC (red fluorescence), respectively.

Chapter 7 Transduction of quantum dots (QDs) and magnetic nanoparticles (TMADM) into ASCs

7.1 Introduction

Recently, magnetic material is noticed that it can be used for biomedical application as bio sensor and diagnosis. bio-imaging, cell separation, drug delivery and gene delivery used nano-particle are studied. Especially, bio medical approaches such as imaging used fluorescence quantum dots nano-particle which is uptake into cells and observed from outside body are studied.

In previous study, Oishi *et al.* recently developed six kinds of novel cationic nanoparticles^{32,65} and found that cells were efficiently labeled with one of the positively-charged nanoparticles. The trimethylamino dextran-coated magnetic iron oxide nanoparticle (TMADM) could be used for labeling adipose tissue-derived stem cells (ASCs) as a contrast agent *in vitro*³². The labeled ASCs could be imaged with good contrast using a 1T MR imaging system. However, this method is difficult to observe the single cells due to MR resolution.

In this study, I combine TMADM and QDs for multi modal imaging with high resolution identification. In this chapter, I demonstrated the transduction efficiency of TMADM and the influence of QDs-TMADM labeling on the properties of ASC.

7.2 Materials and methods

7.2.1 The transduction efficiency of QDs-TMADM to ASCs

Qdot ITK Carboxyl Quantum dots (QDs) and Hank's balanced salt solution were purchased from Life TechnologiesTM Japan (Tokyo, Japan). Fetal bovine serum (FBS) was purchased from Trace Scientific Ltd. (Melbourne, Australia). Magnetic iron oxide nanoparticles (TMADM) was synthesized and purchased from Cosmo Bio[®] Japan (Tokyo, Japan)(Fig. 12A). Collagenase Type II was purchased from Koken Co., Ltd. (Tokyo, Japan).. Non-luminescence feed without alfalfa was purchased from SLC Japan, Inc. (Tokyo, Japan). Cell Counting Kit-8 (CCK-8) was purchased from DOJINDO Laboratories (Kumamoto, Japan).

QDs (2 nM) and TMADM (0, 7.5, 30, 60, 300 $\mu\text{g-Fe/ml}$) were mixed for 15 min at room temperature in order to determine the optimal concentration ratio of QDs/TMADM to transduce into ASCs. ASCs were incubated with the QDs-TMADM in a transduction medium at 37°C. After 4 h incubation, the cells were washed using

transduction medium. Then, the transduction of QDs-TMADM-03 into ASCs were observed by phase-contrast fluorescence microscopy. The transduction efficiency was evaluated by flow cytometry analysis (BD LSRFortessa™ X-20, Japan BD, Tokyo, Japan). Iron content of ASCs were determined by phenanthroline absorptiometry.

7.2.2 Fluorescence and TEM analysis.

QDs (2 nM) and TMADM (60 µg-Fe/ml) were mixed for 15 min at room temperature for inducing transduction into ASCs. ASCs were incubated with R8-ZZC in a transduction medium at 37°C. After 1 h incubation, the cells were washed using transduction medium. The transduction of ZZC into ASCs was the observed by fluorescence image and TEM image. The transduction of QDs-TMADM into ASCs was the observed by phase-contrast fluorescence microscopy. Transmission electron microscopy (TEM, H-7650, Hitachi, Japan) was used to visualize the QDs-TMADM nanoparticles in ASCs at an accelerating voltage of 100 kV.

7.2.3 The cytotoxicity of QDs-TMADM to ASCs

ASCs (1×10^4 cells) were seeded in a 96-well plate (BD Falcon; BD Biosciences,) with 100 µl of culture medium, and the cells were cultured for 24 h. QDs (0, 2, 4, 8, 16, 24 nM) and TMADM (0, 60, 120, 240, 480, 960 µg-Fe/mL) were mixed severally, and QDs-TMADM were transduced into ASCs in a transduction medium (DMEM/F12 containing 2% FBS and 100 U/mL penicillin/streptomycin). After 4 h transduction, ASCs were washed twice by a transduction medium, and were incubated for 24 h. After that, viable cells were counted using Cell Counting Kit-8 (CCK-8). CCK-8 reagent (10 µL) was added to each well and the reaction was allowed to proceed for 2 h. The absorbance of the sample at 450 nm was measured against a background control using a microplate reader (POLARstar OPTIMA; BMG LABTECH, Ortenberg, Germany).

7.2.4 The proliferation of ASCs labeled with QDs-TMADM

ASCs (4×10^3 cells) were seeded in 96-well plate with 100 µL of culture medium for 1 day. QDs (0, 0.2, 0.4, 2, 4 nM) and TMADM (0, 6, 12, 60, 120 µg-Fe/mL) were mixed, and then each complex was transduced into ASCs for 4 h. Then, the cells were washed and the medium was replaced with 100 µL of new culture medium. After 2

and 4 days, viable cells were counted using the CCK-8 in the same way as the cytotoxic method.

7.3 Results and discussion

7.3.1 The optimal concentration ratio of QDs and TMADM

To investigate the optimal concentration ratio of QDs and TMADM for the labeling of ASCs, 2.0 nM of QDs was mixed with various concentrations of TMADM (0, 7.5, 30, 45, 60 and 300 μ M), and these complexes were transduced into ASCs for 12 h. The red fluorescence of QDs-labeled ASCs could be detected when the TMADM concentration of more than 7.5 μ M were used (Fig. 12B-b, d, f, h, j, l). The labeling efficiency and fluorescence intensity of QDs conjugated to TMADM for ASCs were 59.5% (60 μ M TMADM), and 65.0% (300 μ M TMADM), respectively (Fig. 12C). The content of TMADM in the ASCs were determined by phenanthroline absorptiometry (Fig.12D). These data suggest that the optimal concentration ratio of QDs to TMADM is 1 nM : 30 μ g-Fe/ml.

7.3.2 The evaluation of ASCs labeled with QDs-TMADM

To investigate the intracellular distribution of QDs conjugated TMADM, fluorescence image and TEM image of QDs and TMADM are shown in Fig. 13A and 13B. QDs-TMADM were transduced into ASCs for 1 h. The red fluorescence derived from QDs was able to be observed in cytoplasm, and aggregation of QDs was also observed (Fig.13A-c,d). In the TEM image, TMADM was observed in cytoplasm and lysosomes (Fig.13B-b,c). Furthermore, the surface of ASCs was found to be covered with TMADM (Fig.13B-d). These data suggest that TMADM could be transduced into ASCs within one hour of incubation.

To examine the cytotoxicity of QDs-TMADM, various concentrations (0, 2.0, 4.0, 8.0, 16 and 24 nM) of QDs were transduced into ASCs using TMADM (0, 60, 120, 240, 480, 960 μ g-Fe/mL) for 4 h at the optimal ratio, and the ASCs were incubated for 24 h. More than 95% of the ASCs were confirmed to be alive in the QDs concentration of less than or equal to 4 nM. Significant cytotoxicity was observed in the ASCs transduced with 24 nM of QDs, and less than 40% of the cells remained alive (Fig. 13C).

The influence QDs-TMADM on the proliferation rate of ASCs was also examined within the non-cytotoxic range of concentrations. ASCs were confirmed to exhibit a growth rate that was nearly equal to normal ASCs. There were no significant differences at these concentrations of TMADM (Fig. 13D). These data suggest that ASCs can be labeled in QDs concentration of less than or equal to 4 nM with TMADM.

7.4 Conclusion

I demonstrated that TMADM, which is a positive charged magnetic nanoparticle, can label ASCs. Oishi *et al.* have already reported that the zeta voltages of TMADM were +2.0 mV⁶⁶. When ASCs were transduced with TMADM during an hour incubation, the surface of ASCs was observed to be covered with TMADM by TEM imaging. We have already revealed that TMADM is a useful imaging and transduction material of living cells.

The optical complex ratio of QDs and TMADM for ASCs labeling was 1 nM : 30 µg-Fe/ml. The cytotoxicity of QDs-TMADM to ASCs was observed at a concentration of 4 nM. In previous study, the cytotoxicity of CdSe-based QDs was observed at 16 nM¹⁷. It was shown that the cytotoxicity to ASCs was not changed with TMADM.

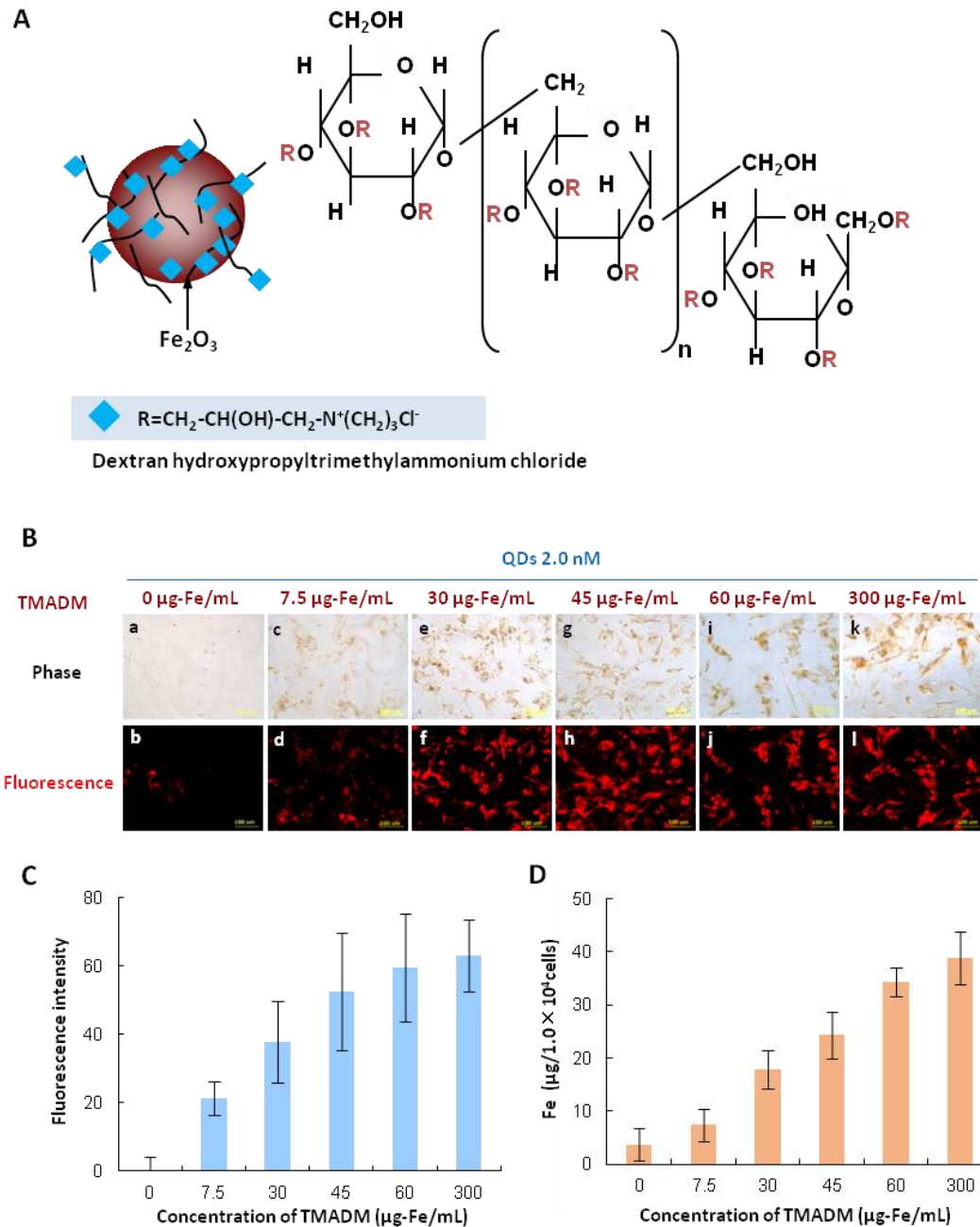


Fig.12 The optimal concentration ratio of QDs and TMADM for labeling ASCs.

A: Schematic illustration of TMADM. B: The phase (a, c, e, g, I, k) and fluorescence (b, d, f, h, j, l) image of mASCs labeled with QDs and various concentrations (0, 7.5, 30, 45, 60, 300 $\mu\text{g-Fe/ml}$) of TMADM complexes. C: Graphs of the labeling efficiency of QDsASCs labeled with QDs (2 nM) and various concentrations (0, 7.5, 30, 45, 60, 300 $\mu\text{g-Fe/ml}$) of TMADM complexes. D: Graphs of the content of transduced TMADM (0, 7.5, 30, 45, 60, 300 $\mu\text{g-Fe/ml}$) into ASCs. The data are shown as the mean \pm SD.

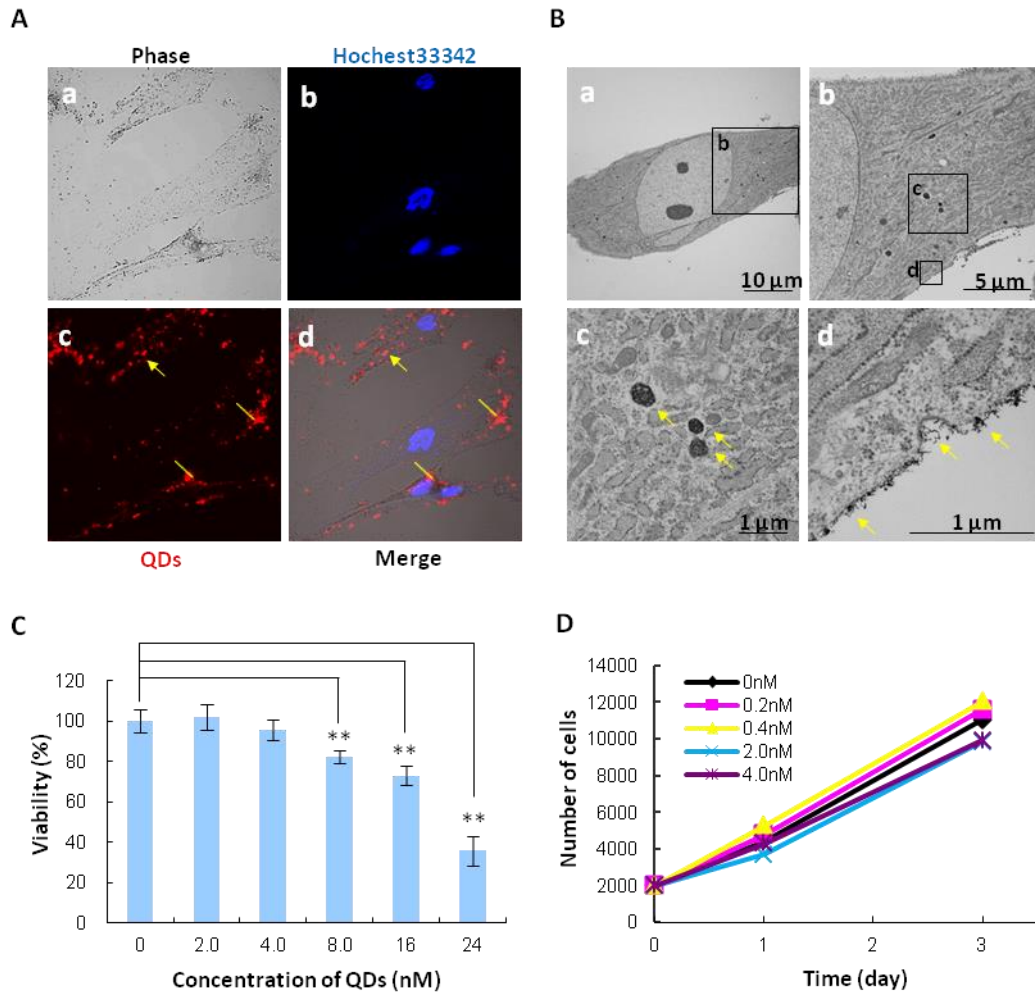


Fig.13 Confirmation of the uptake of TMADM by ASCs and cytotoxicity.

A: Integrated situation of captured QDs and TNADN complexes in the cells. Those pictures show phase (a), nuclear (b), QDs (c) and merge (d) imaging. B: The images obtained by transmission electron microscopy of ASCs labeled with QDs (1 nM) and TMADM (30 $\mu\text{g-Fe/mL}$) complexes for 1 h at 37°C (a–d). A picture of the cells labeled with TMADM is shown (a). The surface of the cells labeled with TMADM is shown (b). The aggregates of the TMADM internalized into ASCs are shown by yellow arrows in (c) and (d). C: The viability of ASCs labeled with QDs and TMADM complexes after a 1 h transduction at 37°C. The data are shown as the mean \pm SD. D: Cell proliferation rate of mASCs transduced various concentration Qds-TMADM at 0, 1 and 3 days after 1 h transduction.

Chapter 8 *In vitro* and *in vivo* imaging of ASCs labeled with QDs-TMADM

8.1 Introduction

Stem cell transplantation has been expected to have applications for regenerative medicine. The identification each transplanted cells is necessary for their clinical applications. In previous chapter, I developed multi modal imaging tools, that could be transduced into ASCs, used by MR and fluorescence imaging. TMADM is a useful imaging and transduction material of living cells. The results from studies introduce a visualization gap between the *in vitro* and *in vivo* studies that, if solved, could enable the early detection of ASCs, the high resolution monitoring of ASCs during treatment, and the greater accuracy in assessment of different imaging agents.

In this chapter, I investigated the usefulness of QDs-TMADM for observation of the transplanted ASCs. To examine QDs-TMADM resolution in the body, *in vivo* imaging of transplanted QDs-TMADM-labeled ASCs was performed in mice using an *in vivo* imaging system. And using different color QDs, I inspected the identification each cell and acquisition of the positional information.

8.2 Materials and methods

8.2.1 *In vitro* imaging of ASCs labeled with QDs-TMADM

QDs-TMADM was transplanted into ASCs for 1 h. The fluorescence image and intensities of ASCs (1×10^5 cells) labeled with QDs (0, 0.5, 1, 2, 4, 8 nM) conjugated TMADM (0, 15, 30, 60, 120, 240 $\mu\text{g-Fe/mL}$) in 1.5 mL tubes were investigated by using IVIS[®] Lumina K Series III (excitation filter: 620 nm \pm 20 nm, emission filter: 670 nm \pm 40 nm). And ASCs labeled with QDs-TMADM were also detected by MR imaging. MR imaging data were collected on a 1T MRI (MRTechnology, Tsukuba, Japan) according to the manufacture's procedure. In brief, the imaging parameters were as follows: T2 sequences with a TR/TE of 3,000/69 ms, field of view (FOV): 30 and two averages were taken for a total acquisition time of about 14 min. T1 sequences were composed of a TR/TE of 500/9 ms, FOV: 30 and four averages for a total acquisition time of about five minutes. All T1 and T2 -weighted image data sets were visually evaluated to identify the location of the transplanted cells within each 1.5 mL tubes.

8.2.2 *In vivo* imaging of ASCs labeled with QDs-TMADM

QDs-TMADM (2 nM QDs and 60 $\mu\text{g-Fe/mL}$ TMADM) was transplanted into ASCs for 1 h. Various numbers of the labeled ASCs (1×10^5 , 5×10^5 , 1×10^6 cells) were transplanted on the backs of mice. The fluorescence images and intensities were investigated using an IVIS Lumina K Series III (excitation filter: $620\text{ nm} \pm 20\text{ nm}$, emission filter: $670\text{nm} \pm 40\text{ nm}$).

The mice were lightly anesthetized using isoflurane (3% induction and 1.5% maintenance) prior to imaging. MR imaging data were collected on a 1T MRI (MRTechnology, Tsukuba, Japan) according to the manufacture's procedure. In brief, the imaging parameters were as follows: T2 sequences with a TR/TE of 3,000/69 ms, field of view (FOV): 30 and two averages were taken for a total acquisition time of about 14 min. T1 sequences were composed of a TR/TE of 500/9 ms, FOV: 30 and four averages for a total acquisition time of about five minutes. All T1 and T2 - weighted image data sets were visually evaluated to identify the location of the transplanted cells within each animal.

8.2.3 Multi color imaging of ASCs labeled with QDs-TMADM

Several wavelength QDs (655, 705, 800 nm) were transduced into ASCs with TMADM (60 $\mu\text{g-Fe/mL}$) for 4 h. labeled ASCs in 1.5 mL tubes were investigated by using IVIS[®] Lumina K Series III (excitation filter: $520\text{ nm} \pm 20\text{ nm}$ (QDs655), $660\text{ nm} \pm 20\text{ nm}$ (QDs705), $710\text{nm} \pm 20\text{ nm}$ (QDs 800), emission filter: $620\text{ nm} \pm 20\text{ nm}$ (QDs655), $710\text{ nm} \pm 20\text{ nm}$ (QDs705), $790\text{nm} \pm 20\text{ nm}$ (QDs 800),). And ASCs labeled with QDs-TMADM were also detected by MR imaging. MR imaging were detected with the same conditions that were used for *in vivo* imaging. Then, these ASCs were transplanted on the backs of mice. The fluorescence images and intensities were investigated using an IVIS Lumina K Series III, and MR image were investigated on a 1T MRI. The mice were lightly anesthetized using isoflurane (3% induction and 1.5% maintenance) prior to MR imaging.

8.3 Results and discussion

8.3.1 *In vitro* imaging of ASCs by magnetic resonance and fluorescence imaging

To examine whether QDs-TMADM-labeled ASCs could be quantitatively detected, various concentration of QDs-TMADM were transduced into ASCs (1.0×10^5 cells). The labeled ASCs were collected in PBS and spun down. The cell pellets were then

prepared for a fluorescence analysis in microtubes (Fig.14A-a). The QDs-TMADM-labeled cell pellets could be quantitatively detected at higher levels of fluorescence intensity more than only QDs- labeled ASCs (Fig 14A-a,b). Moreover, the QDs-TMADM-labeled cell pellets could be also detected by MRI imaging (Fig. 14B). These data suggest that the QDs-TMADM could be detected into labeled cells when the fluorescence intensity was sufficient for cell visualization by fluorescence and MRI imaging.

8.3.2 *In vivo* imaging of ASCs

To assess whether images of transplanted ASCs labeled with QDs-TMADM could be obtained in mice, various numbers of the labeled ASCs (1×10^5 , 5×10^5 , 1×10^6 cells) were transplanted on the backs of mice (Fig. 15A-a,b) . The transplanted QDs-TMADM-labeled ASCs could be detected quantitatively by *in vivo* fluorescence imaging (Fig. 15A-b,c). Moreover, using MRI imaging, these ASCs labeled with QDs-TMADM were detected (Fig. 15B-a,b).

To examine whether TMADM could be also labeled ASCs with different wave length QDs and be detected, TMADM were conjugated QDs655, QDs705 and QDs800. Several QDs-TMADM were transduced into ASCs (Fig. 16A), and the ASCs were transplanted on the backs of mice (Fig.16B-a). The transplanted ASCs labeled with QDs-TMADM could be detected with each wave length QDs by fluorescence imaging (Fig.16B-b), and transplanted areas were detected by MRI imaging (Fig.16B-c).

Those date suggest that TMADM could be detected *in vivo* and changed the fluorescence color easily by mixing QDs.

8.4 Conclusion

The QDs-TMADM-labeled ASCs in the microtube could be quantitatively detected (depending on the number of ASCs) by analyzing the fluorescence intensity using an *in vivo* fluorescence imaging system. The subcutaneously transplanted the QDs-TMADM-labeled ASCs on the backs of mice could also be quantitatively detected. Furthermore, using an MRI system, the QDs-TMADM-labeled ASCs was detected in same areas which I injected ASCs.

And because QDs and TMADM were combined by electrostatic interactions, TMADM can be change the fluorescence color easily. In this study, I conjugate

TMADM with 3 color QDs (QDs655, QDs705 and QDs800). As a results, 3 wave length fluorescence were detected using an *in vivo* fluorescence imaging system and TMADM was detected in same areas using an MRI system.

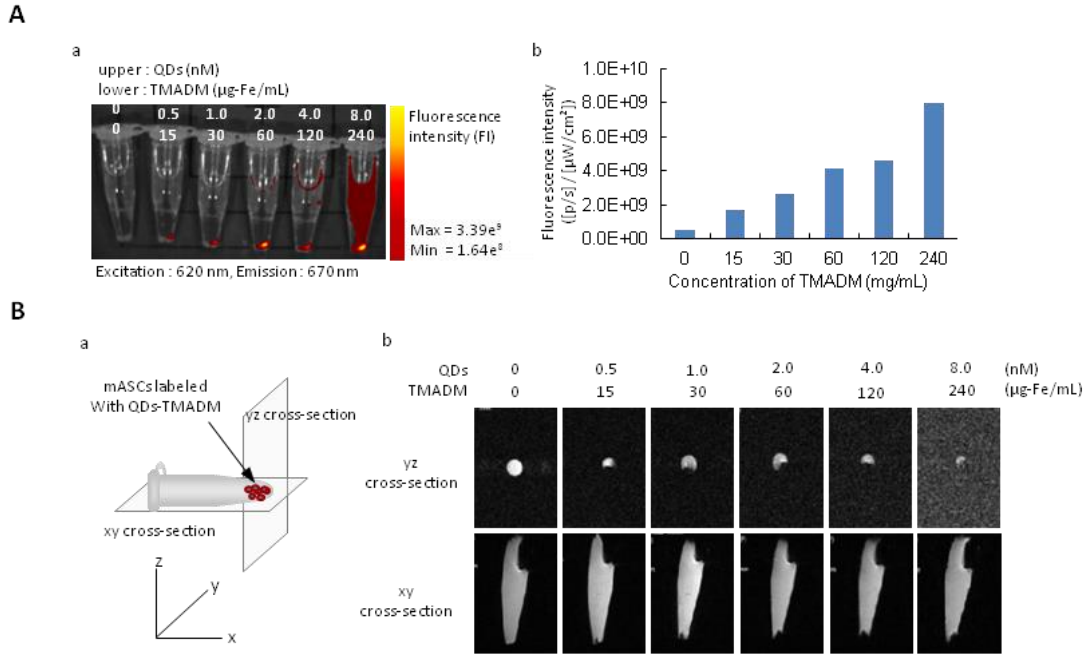


Fig.14 *in vitro* imaging of ASCs labeled with QDs-TMADM.

A: *In vitro* Fluorescence imaging (a) and fluorescence intensity (b) of ASCs (1.0×10^6 cells) labeled with QDs(0, 0.5, 1.0, 2.0, 4.0, 8.0 nM) conjugated with TMADM (15, 30, 60, 120, 240 $\mu\text{g-Fe/mL}$) in 1.5 ml tube.

B: *In vitro* MR imaging of unlabeled and labeled ASCs (1.0×10^6 cells) with various concentration QDs-TMADM (a). yx cross-section (upper) and xy cross-section (lower) weighted images were obtained for unlabeled ASCs and for ASCs labeled with QDs(0, 0.5, 1.0, 2.0, 4.0, 8.0 nM) conjugated with TMADM (15, 30, 60, 120, 240 $\mu\text{g-Fe/mL}$)(b).

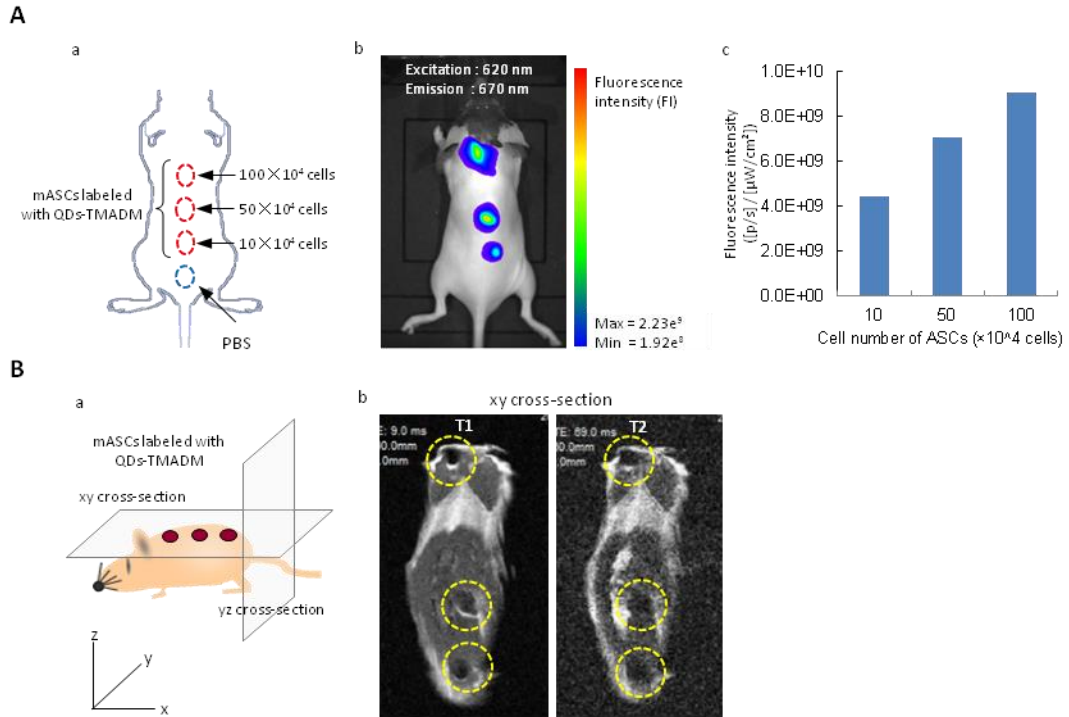


Fig.15 *in vivo* imaging of ASCs labeled with QDs and TMADM complexes.

A: *In vivo* fluorescence imaging of various numbers of ASCs (10×10^4 , 50×10^4 , 100×10^4 cells) labeled with QDs-TMADM (2 nM of QDs) (a,b). Excitation: 620 nm, Emission: 670 nm. The fluorescence intensity were calculated from the fluorescence image(c).

B: *In vivo* MR imaging of the same number of ASCs (1.0×10^6 cells) labeled with QDs-TMADM (2 nM of QDs) in a cross-section figure from the back of the mouse. T1- (left) and T2- (right) weighted images were obtained for ASCs labeled with QDs-TMADM. Yellow dotted circles show the transplanted ASCs (a,b).

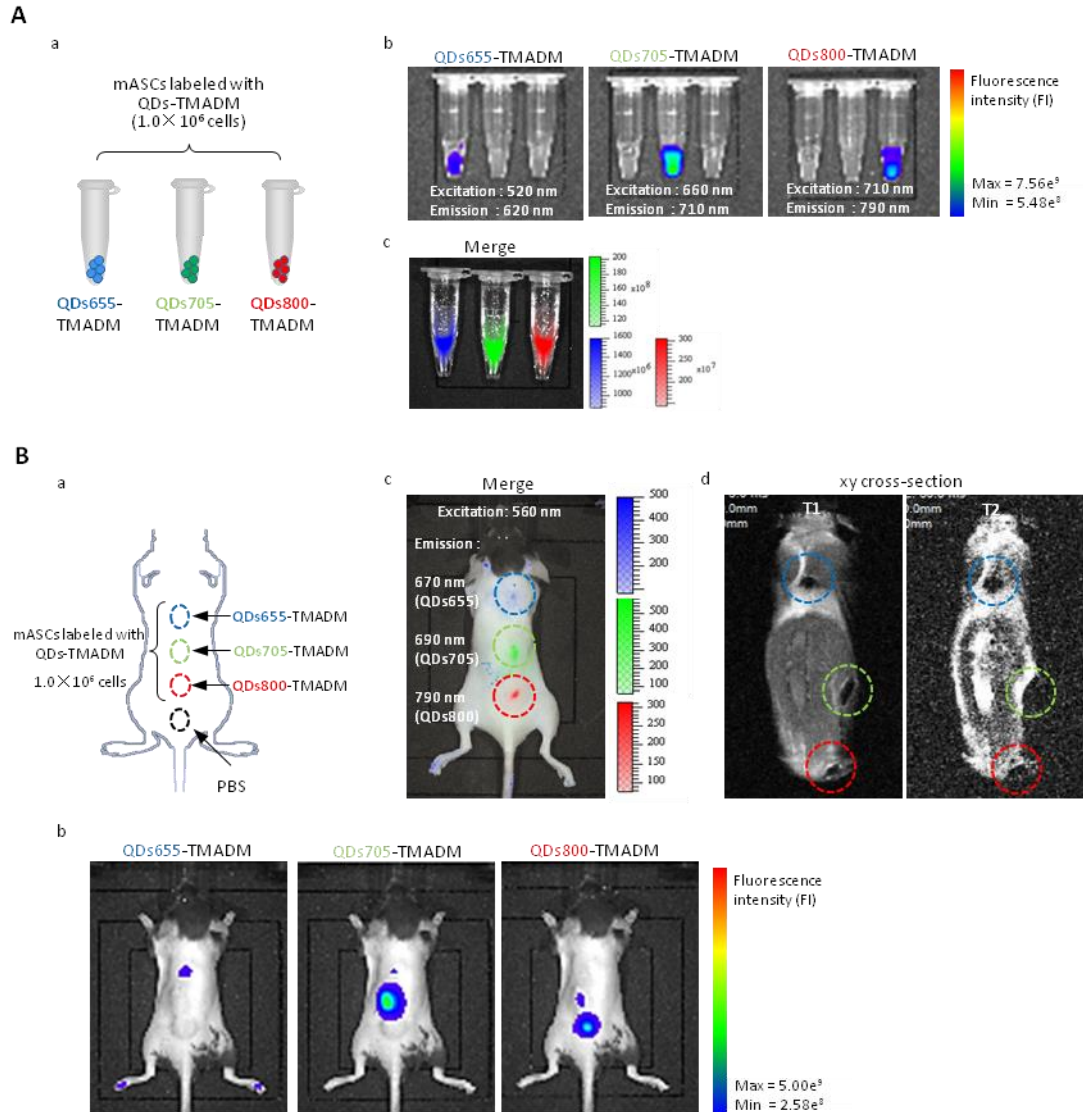


Fig.16 Multi color imaging of ASCs labeled with QDs and TMADM complexes.

A: *In vitro* fluorescence imaging of ASCs (1.0×10^6 cells) labeled with QDs-TMADM. Different color QDs (655, 705, 800 nm) were conjugated with TMADM and transduced into ASCs(a). Fluorescence imaging were acquired by *in vivo* fluorescence imaging system(b,c). **B:** *In vivo* multimodal imaging of ASCs (1.0×10^6 cells) labeled with QDs-TMADM. ASCs labeled with different color QDs (655, 705, 800 nm) and TMADM were transplanted into the back of mice. Fluorescence imaging were acquired by *in vivo* fluorescence imaging system (a,b,c). Excitation: 520 nm (QDs655), 660 nm (QDs705), 710 nm (QDs800); Emission: 620 nm (QDs655), 710 nm (QDs705), 790 nm (QDs800). *In vivo* MR imaging of the same number of ASCs (1.0×10^6 cells) labeled with QDs-TMADM (2 nM of QDs) in a cross-section figure from the back of the mouse(d).T1- (left) and T2- (right) weighted images were

obtained for ASCs labeled with TMADM. Blue, green and red dotted circles show the transplanted ASCs labeled with different color QDs.

Chapter 9 Concluding remarks

In this study, I show the possibility of *in vivo* imaging method for stem cell therapy. The safety of newly synthesized form of aqueous carboxylated ZnS-ZAIS nanoparticles (ZZC) was assessed. ZZC showed strong fluorescence in cell culture medium, and a complex of ZZC and R8 peptides (R8-ZZC) was able to label ASCs with high efficiency. The cytotoxicity of R8-ZZC to ASCs was found to be extremely low in comparison to CdSe-based QDs, and R8-ZZC was not found to influence the proliferation rate or differentiation ability of ASCs. In addition, R8-ZZC did not induce the production of major inflammation cytokines (TNF- α , IFN- γ , IL-12p70, IL-6 and MCP-1) in ASCs. The transplanted R8-ZZC-labeled ASCs could be quantitatively detected in the lungs and liver mainly using an *in vivo* imaging system. The transplanted ASCs were found to aggregate at many sites in the lungs, whereas they were found to individually accumulate in the liver using high-speed multiphoton confocal laser microscopy. These findings suggest that R8-ZZC could be utilized for the labeling and *in vivo* visualization of transplanted ASCs.

Transplanted ASCs labeled with QDs conjugated TMADM (QDs-TMADM) could be detected with fluorescence imaging and MRI. The transplanted ASCs labeled with QDs-TMADM could be detected with 3 colors QDs by fluorescence imaging, and transplanted areas were detected by MRI imaging. Using this multimodal imaging tools, cell transplantation can be more accurate and clearly to detect the cellular kinetics.

This study suggests that novel QDs and magnetic nanoparticle can be used for the labeling and *in vivo* imaging. The findings of the present study are expected to contribute to further progress in their clinical applications.

Acknowledgements

I would like to express appreciation to Professor Yoshinobu Baba (Nagoya University) for his kind guidance, constructive suggestions, simulating discussions and continuous encouragement.

I would like to acknowledge Associate Professor Noritada Kaji, Program-Specific Senior Lecturer Hiroshi Yukawa, Program-Specific Senior Lecturer Daisuke Onoshima, Assistant Professor Takao Yasui (Nagoya University) and Guest Teacher Toshihiro Kasama (Tokyo University) for their valuable suggestions and experimental instruction.

I would like to express my gratitude to all the collaborators : Professor Tetsuya Ishikawa (Nagoya University) for offering Experimental device and mice; Professor Tsukasa Torimoto and Assistant Professor Tatsuya Kameyama (Nagoya University) for synthesis of ZZC nanoparticle; Ichiro Kato (Meito Sangyo Co.,Ltd.) for synthesis of TMADM.

Especially, I appreciate the help of Ms. Yoko Tsutsui and Ms. Tomoko Arimoto (Nagoya University) for the treatment of ASCs.

Thanks to present and former members in professor Baba's laboratory are extended: thank you all for making the lab such a great place to work. Dr. Sakon Rahong, Mr. Sreenadh Sasidharan Pollai, Mr. Abdallah M. Zeid, Ms. sun xiaovin, Mr. Yuki Konakade, Mr. Ryo Koyama, Mr. Masataka Makino, Mr. Hirotohi Yasaki, Mr. Shigetaka Inagaki, Mr. Tomoki Okawa, Ms. Mamiko Sano, Mr. Daiki Takeshita, Ms. Keiko Tabuchi, Mr. Atsunori Hattori, Ms. Shiori Ito, Mr. Taisuke Shimada, Ms. Reina Naruse, Mr. Yuya Hattori, Ms. Asami Yokoyama, Mr. Akihiro Yonese, Mr. Koya Ishikawa, Mr. Daiki Kuboyama, Ms. Kaori Kobayashi, Mr. Yuta Nakamura, Mr. Yosuke Nakamura, Mr. Masashi Hirakawa, Mr. Ivan Adiyasa Thiodorus, Mr. Keita Aoki, Mr. Kentarou Uchida, Mr. Taiki Suzuki, Ms. Sun Mingyue, Mr. Tsuyoshi Naganawa and Mr. Ryou Magofuku.

This research was mainly supported by the Japan Agency for Medical Research and Development (AMED) through its “Research Center Network for Realization of Regenerative Medicine”. This work was partially supported by JSPS KAKENHI Grant Numbers 26790006. And this work was supported by a Grant-in- Aid for the Nagoya University Advanced Leading Graduate Program by the Ministry of Education, Culture, Sports, Science and Technology

(MEXT), Japan.

References

1. Sakaida, I.; Terai, S.; Yamamoto, N.; Aoyama, K.; Ishikawa, T.; Nishina, H.; Okita, K. Transplantation of bone marrow cells reduces CCl₄-induced liver fibrosis in mice. *Hepatology* **40**, 1304-1311 (2004).
2. Banas, A.; Teratani, T.; Yamamoto, Y.; Tokuhara, M.; Takeshita, F.; Osaki, M.; Kawamata, M.; Kato, T.; Okochi, H.; Ochiya, T. IFATS collection: in vivo therapeutic potential of human adipose tissue mesenchymal stem cells after transplantation into mice with liver injury. *Stem Cells* **26**, 2705-2712 (2008).
3. Urbán, V.S.; Kiss, J.; Kovács, J.; Gócza, E.; Vas, V.; Monostori, E.; Uher, F. Mesenchymal stem cells cooperate with bone marrow cells in therapy of diabetes. *Stem Cells* **26**, 244-253 (2008).
4. Bianco, P.; Cao, X.; Frenette, P. S.; Mao, J. J.; Robey, P. G.; Simmons, P. J.; Wang, C. Y. The meaning, the sense and the significance: translating the science of mesenchymal stem cells into medicine. *Nat. Med.* **19**, 35-42 (2013).
5. Bhatia, S.N.; Underhill, G. H.; Zaret, K. S.; Fox, I. J. Cell and tissue engineering for liver disease. *Sci. Transl. Med.* **6**, 245sr2 (2014).
6. Chen, G.; Tian, F.; Li, C.; Zhang, Y.; Weng, Z.; Zhang, Y.; Peng, R.; Wang, Q. *In vivo* real-time visualization of mesenchymal stem cells tropism for cutaneous regeneration using NIR-II fluorescence imaging. *Biomaterials* **53**, 265-273 (2015).
7. Ke, C.; Chen, J.; Guo, Y.; Chen, Z. W.; Cai, J. Migration mechanism of mesenchymal stem cells studied by QD/NSOM. *Biochim. Biophys. Acta.* **1848**, 859-868 (2015).
8. Ding, D.; Mao, D.; Li, K.; Wang, X.; Qin, W.; Liu, R.; Chiam, D. S.; Tomczak, N.; Yang, Z.; Tang, B. Z.; Kong, D.; Liu, B. Precise and long-term tracking of adipose-derived stem cells and their regenerative capacity via superb bright and stable organic nanodots. *ACS Nano* **8**, 12620-12631 (2014).
9. Constantin, G.; Marconi, S.; Rossi, B.; Angiari, S.; Calderan, L.; Anghileri, E.; Gini, B.; Bach, S. D.; Martinello, M.; Bifari, F.; Galiè, M.; Turano, E.; Budui, S.; Sbarbati, A.; Krampera, M.; Bonetti, B. Adipose-derived mesenchymal stem cells ameliorate chronic experimental autoimmune encephalomyelitis. *Stem Cells* **27**, 2624-2635 (2009).
10. Bernal, W.; Auzinger, G.; Dhawan, A.; Wendon, J. Acute liver failure. *Lancet* **376**, 190-201 (2010).

11. Dhawan, A.; Puppi, J.; Hughes, R. D.; Mitry, R. R. Human hepatocyte transplantation: current experience and future challenges. *Nat. Rev. Gastroenterol. Hepatol* **7**, 288-298 (2010).
12. Ichai, P.; Samuel, D. Etiology and prognosis of fulminant hepatitis in adults. *Liver Transpl* **14**,67-79 (2008).
13. Liu, J. H.; Cao, L.; LeCroy, G. E.; Wang, P.; Meziani, M. J.; Dong, Y.; Liu, Y.; Luo, P. G.; Sun, Y. P. Carbon "quantum" dots for fluorescence labeling of cells. *ACS Appl. Mater. Interfaces* **7**, 19439-19445 (2015).
14. Han, H. S.; Niemeyer, E.; Huang, Y.; Kamoun, W. S.; Martin, J. D.; Bhaumik, J.; Chen, Y.; Roberge, S.; Cui, J.; Martin, M. R.; Fukumura, D.; Jain, R. K.; Bawendi, M. G.; Duda, D. G. Quantum dot/antibody conjugates for *in vivo* cytometric imaging in mice. *Proc. Natl. Acad. Sci. U.S.A.* **112**, 1350-1355 (2015).
15. Park, J. S.; Yi, S. W.; Kim, H. J.; Kim, S. M.; Shim, S. H.; Park, K. H. Sunflower-type nanogels carrying a quantum dot nanoprobe for both superior gene delivery efficacy and tracing of human mesenchymal stem cells. *Biomaterials* **77**, 14-25 (2016).
16. Yukawa, H.; Mizufune, S.; Mamori, C.; Kagami, Y.; Oishi, K.; Kaji, N.; Okamoto, Y.; Takeshi, M.; Noguchi, H.; Baba, Y.; Hamaguchi, M.; Hamajima, N.; Hayashi, S. Quantum dots for labeling adipose tissue-derived stem cells. *Cell Transplant* **18**, 591-599 (2009).
17. Yukawa, H.; Kagami, Y.; Watanabe, M.; Oishi, K.; Miyamoto, Y.; Okamoto, Y.; Tokeshi, M.; Kaji, N.; Noguchi, H.; Ono, K.; Sawada, M.; Baba, Y.; Hamajima, N.; Hayashi, S. Quantum dots labeling using octa-arginine peptides for imaging of adipose tissue-derived stem cells. *Biomaterials* **31**, 4094-4103 (2010).
18. Soenen, S. J.; Manshian, B. B.; Aubert, T.; Himmelreich, U.; Demeester, J.; De Smedt, S. C.; Hens, Z.; Braeckmans, K. Cytotoxicity of cadmium-free quantum dots and their use in cell bioimaging. *Chem. Res. Toxicol.* **27**, 1050-1059 (2014).
19. Shang, W.; Zhang, X.; Zhang, M.; Fan, Z.; Sun, Y.; Han, M.; Fan, L. The uptake mechanism and biocompatibility of graphene quantum dots with human neural stem cells. *Nanoscale* **6**, 5799-5806 (2014).
20. Liu, T.; Xing, R.; Zhou, Y. F.; Zhang, J.; Su, Y. Y.; Zhang, K. Q.; He, Y.; Sima, Y. H.; Xu, S. Q. Hematopoiesis toxicity induced by CdTe quantum dots determined in an invertebrate model organism. *Biomaterials* **35**, 2942-2951 (2014).

21. Deng, D.; Cao, J.; Qu, L.; Achilefu, S.; Gu, Y. Highly luminescent water-soluble quaternary Zn-Ag-In-S quantum dots for tumor cell-targeted imaging. *Phys. Chem. Chem. Phys.* **15**, 5078-5083 (2013).
22. Torimoto, T.; Adachi, T.; Okazaki, K.; Sakuraoka, M.; Shibayama, T.; Ohtani, B.; Kudo, A.; Kuwabata, S. Facile synthesis of ZnS-AgInS₂ solid solution nanoparticles for a color-adjustable luminophore. *J. Am. Chem. Soc.* **129**, 12388-12389 (2007).
23. Torimoto, T.; Ogawa, S.; Adachi, T.; Kameyama, T.; Okazaki, K.; Shibayama, T.; Kudo, A.; Kuwabata, S. Remarkable photoluminescence enhancement of ZnS-AgInS₂ solid solution nanoparticles by post-synthesis treatment. *Chem. Commun (Camb)*. **46**, 2082-2084 (2010).
24. Song, J.; Jiang, T.; Guo, T.; Liu, L.; Wang, H.; Xia, T.; Zhang, W.; Ye, X.; Yang, M.; Zhu, L.; Xia, R.; Xu, X. Facile synthesis of water-soluble Zn-doped AgIn₅S₈/ZnS core/shell fluorescent nanocrystals and their biological application. *Inorg. Chem.* **54**, 1627-1633 (2015).
25. Shinchi, H.; Wakao, M.; Nagata, N.; Sakamoto, M.; Mochizuki, E.; Uematsu, T.; Kuwabata, S.; Suda, Y. Cadmium-free sugar-chain-immobilized fluorescent nanoparticles containing low-toxicity ZnS-AgInS₂ cores for probing lectin and cells. *Bioconjug. Chem.* **25**, 286-295 (2014).
26. Regulacio, M. D.; Win, K. Y.; Lo, S. L.; Zhang, S. Y.; Zhang, X.; Wang, S.; Han, M. Y.; Zheng, Y. Aqueous synthesis of highly luminescent AgInS₂-ZnS quantum dots and their biological applications. *Nanoscale* **5**, 2322-2327 (2013).
27. Luo, Z.; Zhang, H.; Huang, J.; Zhong, X. One-step synthesis of water-soluble AgInS₂ and ZnS-AgInS₂ composite nanocrystals and their photocatalytic activities. *J. Colloid Interface Sci.* **377**, 27-33 (2012).
28. Nohroudi K.; Arnhold, S.; Berhorn, T.; Addicks, K.; Hoehn, M.; Himmelreich, U. *In vivo* MRI stem cell tracking requires balancing of detection limit and cell viability. *Cell transplant.* **19**, 431-441 (2010).
29. Gerben M.; Kotek, G.; Wielopolski, P. A.; Farrell, E.; Bos, P. K.; Weinans, H.; Grohnert, A. U.; Jahr, H.; Verhaar, J. A.; Krestin, G. P.; van Osch, G. J.; Bernsen, M. R. Clinically translatable cell tracking and quantification by MRI in cartilage repair using superparamagnetic iron oxides. *PLOS ONE*. **6**, e17001 (2011).
30. Kim TH.; Kim, J. K.; Shim, W.; Kim, S. Y.; Park, T. J.; Jung, J. Y. Tracking of transplanted mesenchymal stem cells labeled with fluorescent magnetic

- nanoparticle in liver cirrhosis rat model with 3-T MRI. *Magn Reson Imaging*. **28**, 1004-1013 (2010).
31. Xiaoya H.; Jinhua, C.; Bo, L.; Yi, Z.; Yong, Q.; Cellular magnetic resonance imaging contrast generated by the ferritin heavy chain genetic reporter under the control of a Tet-On switch. *Stem Cell Res Ther*. **6**, 207 (2015).
 32. Oishi, K.; Noguchi, H.; Saito, H.; Yukawa, H.; Miyamoto, Y.; Ono, K.; Murase, K.; Sawada, M.; Hayashi, S. Novel positivecharged nanoparticles for efficient magnetic resonance imaging of islet transplantation. *Cell Med*. **3**, 43–49 (2012).
 33. Miyamoto, Y.; Koshidaka, Y.; Noguchi, H.; Oishi, K.; Saito, H.; Yukawa, H.; Kaji, N.; Ikeya, T.; Suzuki, S.; Iwata H.; Baba, Y.; Murase, K.; Hayashi, S. Observation of Positively Charged Magnetic Nanoparticles Inside HepG2 Spheroids Using Electron Microscopy. *Cell Medicine*. **9**, 89-96 (2013)
 34. Yukawa, H.; Nakagawa, S.; Yoshizumi, Y.; Watanabe, M.; Saito, H.; Miyamoto, Y.; Noguchi, H.; Oishi, K.; Ono, K.; Sawada, M.; Kato, I.; Onoshima, D.; Obayashi, M.; Hayashi, Y.; Kaji, N.; Ishikawa, T.; Hayashi, S.; Baba, Y. Novel positively charged nanoparticle labeling for *in vivo* imaging of adipose tissue-derived stem cells. *PLOS ONE*. **9**, e110142 (2014)
 35. Banas, A.; Teratani, T.; Yamamoto, Y.; Tokuhara, M.; Takeshita, F.; Osaki, M.; Kato, T.; Okochi, H.; Ochiya, T. Rapid hepatic fate specification of adipose-derived stem cells and their therapeutic potential for liver failure. *J. Gastroenterol. Hepatol*. **24**,70-77 (2009).
 36. Campagnoli, C.; Roberts, I. A.; Kumar, S.; Bennett, P. R.; Bellantuono, I.; Fisk, N. M. Identification of mesenchymal stem/progenitor cells in human first-trimester fetal blood, liver, and bone marrow. *Blood*. **98**, 2396-402 (2001).
 37. Caplan, A. I.; Dennis, J. E. Mesenchymal stem cells as trophic mediators. *J Cellular Physiol*. **98**, 1076-1084 (2006).
 38. Huss, R. Isolation of primary and immortalized CD34-hematopoietic and mesenchymal stem cells from various sources. *Stem Cells*. **18**, 1-9 (2000).
 39. Jackson, L.; Jones, D. R.; Scotting, P.; Sottile, V. Adult mesenchymal stem cells: differentiation potential and therapeutic applications. *J. Postgrad Med*. **53**,121-7 (2007).
 40. Meirelles, L. D.; Nardi, N. B. Methodology, biology and clinical applications of mesenchymal stem cells. *Front. Biosci*. **14**, 4281-4298 (2009).
 41. Pittenger, M. F.; Mackay, A. M.; Beck, S. C.; Jaiswal, R. K.; Douglas, R.; Mosca,

- J. D.; Moorman, M. A.; Simonetti, D. W.; Craig, S.; Marshak, D. R. Multilineage potential of adult human mesenchymal stem cells. *Science*. **284**, 143-147 (1999).
42. Puissant, N.; Barreau, C.; Bourin, P.; Clavel, C.; Corre, J.; Bousquet, C.; Taureau, C.; Cousin, B.; Abbal, M.; Laharrague, P.; Penicaud, L.; Casteilla, L.; Blancher, A. Immunomodulatory effect of human adipose tissue-derived adult stem cells: comparison with bone marrow mesenchymal stem cells. *Br. J. Haematol.* **129**, 118-129 (2005).
43. Spaggiari, G. M.; Capobianco, A.; Abdelrazik, H.; Becchetti, F.; Mingari, M. C.; Moretta, L. Mesenchymal stem cells inhibit natural killer-cell proliferation, cytotoxicity, and cytokine production: role of indoleamine 2,3-dioxygenase and prostaglandin E2. *Blood*. **111**,1327-1333 (2008).
44. Traktuev, D. O.; Merfeld-Clauss, S.; Li, J.; Kolonin, M.; Arap, W.; Pasqualini, R.; Johnstone, B. H.; March, K. L. A population of multipotent CD34-positive adipose stromal cells share pericyte and mesenchymal surface markers, reside in a periendothelial location, and stabilize endothelial networks. *Circ. Res.* **102**, 77-85 (2008).
45. Yukawa, H.; Watanabe, M.; Kaji, N.; Okamoto, Y.; Tokeshi, M.; Miyamoto, Y.; Noguchi, H.; Baba, Y.; Hayashi, S. Monitoring transplanted adipose tissue-derived stem cells combined with heparin in the liver by fluorescence imaging using quantum dots. *Biomaterials*. **33**, 2177–2186 (2012).
46. Liu, G. T.; Li, Y.; Wei, H. L.; Zhang, H.; Xu, J. Y.; Yu, L. H. Mechanism of protective action of bicyclol against CCl4-induced liver injury in mice. *Liver International*. **25**, 872–879 (2005).
47. Tsutsui, H.; Matsui, K.; Kawada, N.; Hyodo, Y.; Hayashi, N.; Okamura, H.; Higashino, K.; Nakanishi, K. IL-18 accounts for both TNF- α and Fas Ligand-mediated hepatotoxic pathways in endotoxin-induced liver injury in mice. *J. Immunol.* **159**, 3961-3967 (1997).
48. Wong, F. W.; Chan, W. Y.; Lee, S. S. Resistance to carbon tetrachloride-induced hepatotoxicity in mice which lack CYP2E1 expression. *Toxicol. Appl. Pharmacol.* **153**, 109-118 (1998).
49. Yamanaka, A.; Hamano, S.; Miyazaki, Y.; Ishii, K.; Takeda, A.; Mak, T. W.; Himeno, K.; Yoshimura, A.; Yoshida, H. Hyperproduction of proinflammatory cytokines by WSX-1-deficient NKT cells in concanavalin A-induced hepatitis. *J. Immunol.* **172**, 3590-3596 (2004).

50. Yokoyama, M.; Yokoyama, A.; Mori, S.; Takahashi, H. K.; Yoshino, T.; Watanabe, T.; Watanabe, T.; Ohtsu, H.; Nishibori, M. Inducible histamine protects mice from P.acnes-primed and LPS-induced hepatitis through H2-receptor stimulation. *Gastroenterology*. **127**, 892–902 (2004).
51. Iwashima, S.; Ozaki, T.; Maruyama, S.; Saka, Y.; Kobori, M.; Omae, K.; Yamaguchi, H.; Niimi, T.; Toriyama, K.; Kamei, Y.; Torii, S.; Murohara, T.; Yuzawa, Y.; Kitagawa, Y.; Matsuo, S. Novel culture system of mesenchymal stromal cells from human sub- cutaneous adipose tissue. *Stem Cells Dev*. **18**, 533-543 (2009).
52. Kubo, N.; Narumi, S.; Kijima, H.; Mizukami, H.; Yagihashi, S.; Hakamada, K.; Nakane, A. Efficacy of adipose tissue-derived mesenchymal stem cells for fulminant hepatitis in mice induced by concanavalin A. *J. Gastroenterol. Hepatol*. **27**, 165–172 (2012).
53. Mizuhara, H.; Kuno, M.; Seki, N.; Yu, W. G.; Yamaoka, M.; Yamashita, M.; Ogawa, T.; Kaneda, K.; Fujii, T.; Senoh, H.; Fujiwara, H. Strain difference in the induction of T-cell activation-associated, interferon gamma-dependent hepatic injury in mice. *Hepatology*. **27**, 513-519 (1998).
54. Comporti, M. Three models of free radical-induced cell injury. *Chem Biol Interact*. **72**, 1-56 (1989).
55. Kato, J.; Okamoto, T.; Motoyama, H.; Uchiyama, R.; Kirchhofer, D.; Van Rooijen, N.; Enomoto, H.; Nishiguchi, S.; Kawada, N.; Fujimoto, J.; Tsutsui, H. Interferon gamma-mediated tissue factor expression contributes to T cell-mediated hepatitis via induction of hypercoagulation in mice. *Hepatology*. **57**, 362-372 (2013).
56. Baer, P. C.; Geiger, H. Adipose-derived mesenchymal stromal/stemcells: tissue localization, characterization, and heterogeneity. *Stem Cells Int*. **812693**, 1-11 (2012).
57. Zhang, X.; Semon, J. A.; Zhang, S.; Strong, A. L.; Scruggs, B. A.; Gimble, J. M.; Bunnell, B. A. Characterization of adipose-derived stromal/stem cells from the twitcher mouse model of Krabbe disease. *BMC Cell Biology*. **14**, 20-30 (2013).
58. Zhang, S.; Danchuk, SD.; Imhof, K. M.; Semon, J. A.; Scruggs, B. A.; Bonvillain, R. W.; Strong, A. L.; Gimble, J. M.; Betancourt, A. M.; Sullivan, D. E.; Bunnell, B. A. Comparison of the therapeutic effects of human and mouse adipose-derived stem cells in a murine model of lipopolysaccharide-induced acute lung injury.

Stem Cell Res. Ther. **4**, 13-25 (2013).

59. Saka, Y.; Furuhashi, K.; Katsuno, T.; Kim, H.; Ozaki, T.; Iwasaki, K.; Haneda, M.; Sato, W.; Tsuboi, N.; Ito, Y.; Matsuo, S.; Kobayashi, T.; Maruyama, S. Adipose-derived stromal cells cultured in a low-serum medium, but not bone marrow-derived stromal cells, impede xenoantibody production. *Xenotransplantation* **18**, 196-208 (2011).
60. Fang, X.; Wang, R.; Ma, J.; Ding, Y.; Shang, W.; Sun, Z. Ameliorated conA-induced hepatitis in the absence of PKC-theta. *PLOS ONE* **7**, 2:e31174 (2012).
61. Gump, J.M.; June, R. K.; Dowdy, S. F. Revised role of glycosaminoglycans in TAT protein transduction domain-mediated cellular transduction. *J. Biol. Chem.* **285**, 1500-1507 (2010).
62. Cahill, K. Molecular electroporation and the transduction of oligoarginines. *Phys. Biol.* **7**, 16001 (2009).
63. Ho, C. C.; Luo, Y. H.; Chuang, T. H.; Yang, C. S.; Ling, Y. C.; Lin, P. Quantum dots induced monocyte chemotactic protein-1 expression via MyD88-dependent Toll-like receptor signaling pathways in macrophages. *Toxicology* **308**, 1-9 (2013).
64. Zhou, D.; Li, Y.; Hall, E. A.; Abell, C.; Klenerman, D. A chelating dendritic ligand capped quantum dot: preparation, surface passivation, bioconjugation and specific DNA detection. *Nanoscale* **3**, 201-211 (2011).
65. Oishi, K.; Noguchi, H.; Saito, H.; Yukawa, H.; Miyamoto, Y.; Murase, K.; Hayashi, S. Cell labeling with a novel contrast agent of magnetic resonance imaging. *Cell Transplant.* **19**, 887–892 (2010).
66. Oishi, K.; Miyamoto, Y.; Saito, H.; Murase, K.; Ono, K.; Sawada, M.; Watanabe, M.; Noguchi, Y.; Fujiwara, T.; Hayashi, S.; Noguchi, H. In vivo imaging of transplanted islets labeled with a novel cationic nanoparticle. *PLOS ONE.* **8**, e57046 (2013)

List of publications

1. Ogihara Y.; Yukawa H.; Kameyama T.; Nishi H.; Onoshima D.; Ishikawa T.; Torimoto T.; Baba Y., Labeling and *in vivo* visualization of transplanted adipose tissue-derived stem cells with safe cadmium-free aqueous ZnS coating of ZnS-AgInS₂ nanoparticles. *Sci. Rep.*, in press
2. Yoshizumi Y.; Yukawa H.; Iwaki R.; Fujinaka S.; Kanou A.; Kanou Y.; Yamada T.; Nakagawa S.; Ohara T.; Nakagiri K.; Ogihara Y.; Tsutsui Y.; Hayashi Y.; Ishigami M.; Baba Y.; Ishikawa T., Immunomodulatory effects of adipose Tissue-derived stem cells on Concanavalin A-induced acute liver injury in mice. *Cell Medicine.*, inpress
3. Ogihara Y.; Yukawa H.; Onoshima D.; Baba Y., Transduction Function of a Magnetic Nanoparticle TMADM for Stem Cell Imaging with Quantum Dots. *Anal. sci.* , inpress

List of abbreviations

Adipose-derived stem cells (ASCs)
Alanine aminotransferase (ALT)
Alkali-treated dextran-coated magnetic iron oxide nanoparticle (ATDM)
Allophycocyanin (APC)
Bromodeoxyuridine (BrdU)
C–X–C motif chemokine 12 (CXCL12)
Carbon tetrachloride (CCl₄)
Cell counting kit-8 (CCK-8)
Concanavalin A (Con A)
Dulbecco's modified Eagle's medium (DMEM)
Embryonic stem cells (ES cells)
Enzyme-linked immunosorbent assay (ELISA)
Fetal bovine serum (FBS)
Fibroblast growth factor-2 (FGF-2)
Fluorescein isothiocyanate (FITC)
Fluorescence activate cell sorter (FACS)
Fulminant hepatic failure (FHF)
Glyceraldehyde 3-phosphate dehydrogenase (GAPDH)
Hank's balanced salt solution (HBSS)
Hepatocyte growth factor (HGF)
Indoleamine 2, 3-dioxygenase (IDO)
Induced pluripotent stem cells (iPS cells)
Inducible nitric oxide synthase (iNOS)
Insulin, transferrin, selenium (ITS)
Interferon- γ (IFN- γ)
Interleukin (IL)
Lipopolysaccharide (LPS)
Lymphomononuclear cells (LMCs)
Magnetic resonance imaging (MRI)
Mesenchymal stem cells (MSCs)
Myeloid differentiation factor (MD)
Natural killer T (NKT)
Octa-arginine (R8)

Phorbol 12-myristate 13-acetate (PMA)
Phosphate buffered saline (PBS)
Photonic multichannel analyzer (PMA)
Phycoerythrin (PE)
Prostaglandin E2 (PGE2)
Protein kinase C (PKC)
Quantitative real-time reverse-transcription polymerase chain reaction (qRT-PCR)
Quantum dots (QDs)
Region of intensity (ROI)
Roswell Park Memorial Institute (RPMI)
Stromal cell-derived factor (SDF)
Tissue factor (TF)
Toll-like receptor (TLR)
Transforming growth factor (TGF)
Transmission electron microscopy (TEM)
Trimethylamino dextran-coated magnetic iron oxide nanoparticles (TMADM)
Tumor necrosis factor- α (TNF- α)
Vascular endothelial growth factor (VEGF)
ZnS-AgInS₂ (ZAIS)
ZnS-coated ZAIS (ZnS-ZAIS)
ZnS-ZAIS carboxylated nanoparticles (ZZC)